

## Optic issues in ongoing ERL projects

S.L. Smith<sup>a,\*</sup>, B.D. Muratori<sup>a</sup>, H.L. Owen<sup>a</sup>, G.H. Hoffstaetter<sup>b</sup>, V.N. Litvinenko<sup>c</sup>, I. Ben-Zvi<sup>c</sup>, M. Bai<sup>c</sup>, J. Beebe-Wang<sup>c</sup>, M. Blaskiewicz<sup>c</sup>, R. Calaga<sup>c</sup>, W. Fischer<sup>c</sup>, X.Y. Chang<sup>c</sup>, D. Kayran<sup>c</sup>, J. Kewisch<sup>c</sup>, W.W. MacKay<sup>c</sup>, C. Montag<sup>c</sup>, B. Parker<sup>c</sup>, V. Ptitsyn<sup>c</sup>, T. Roser<sup>c</sup>, A. Ruggiero<sup>c</sup>, T. Satogata<sup>c</sup>, B. Surrow<sup>e</sup>, S. Tepikian<sup>c</sup>, D. Trbojevic<sup>c</sup>, V. Yakimenko<sup>c</sup>, S.Y. Zhang<sup>c</sup>, Ph. Piot<sup>d</sup>

<sup>a</sup>*CCLRC Daresbury Laboratory, Keckwick Lane, Daresbury, Warrington WA4 4AD, UK*

<sup>b</sup>*Cornell University, Ithaca, NY, USA*

<sup>c</sup>*BNL, Upton, NY 11973, USA*

<sup>d</sup>*Fermi National Accelerator Laboratory, Batavia, IL 60510, USA*

<sup>e</sup>*Massachusetts Institute of Technology, Department of Physics, Cambridge, MA 02139, USA*

Available online 15 December 2005

### Abstract

A wide range of optics issues for energy recovery linac (ERL)-based projects are illustrated through the presentation of ongoing projects covering both light sources, at Cornell and Daresbury and high energy and nuclear physics accelerators at the Brookhaven National Laboratory. This presented range of projects demonstrates how the different design teams see the challenges of studying and solving optics issues for their particular project's ERLs, with studies appropriate to the stage of maturity of the project. Finally, as an illustration of the complexity and detail behind a single aspect of ERL optics design we present an overview of the highly important generic topic of longitudinal phase space evolution in ERLs.

© 2005 Elsevier B.V. All rights reserved.

PACS: 29.27.-a; 29.27.Bd; 29.27.Eg

Keywords: Energy recovery; Recirculating linacs; Instabilities; Free-electron lasers; Optics

### 1. Introduction

There are many ongoing projects which can be used to illustrate the challenges of optics issues for energy recovery linacs (ERLs). Fig. 1 illustrates the range of some of the ongoing projects worldwide. It shows how very wide consideration is now being given to the use of the ERL principle to achieve intense, high-quality electron beams for a diverse range of applications. In this paper, we take examples from each of the categories of projects and discuss the designs and optics issues relevant to those projects. Across each of the designs there are a number of generic optics issues such as designing to minimize disruptive space charge effects, coherent synchrotron radiation (CSR) and beam breakup

(BBU) instability, etc. Perhaps one of the most important of these issues, given the applications of these accelerators, is the control of the longitudinal dynamics. Only through a deep understanding of the principles and issues in this area can optics designs, which will deliver the high-quality beams to the various projects, be properly conceived. It is this generic topic that we have chosen to review in detail towards the end of this paper.

### 2. Optics issues for the fourth-generation light source (4GLS) project

#### 2.1. Introduction to the 4GLS project

We have used the 4GLS project to illustrate the optic issues being actively considered for this relatively low-energy light source during a feasibility design phase. 4GLS

\*Corresponding author. Tel.: +44 1925 603588; fax: +44 1925 603124.  
E-mail address: [s.l.smith@dl.ac.uk](mailto:s.l.smith@dl.ac.uk) (S.L. Smith).

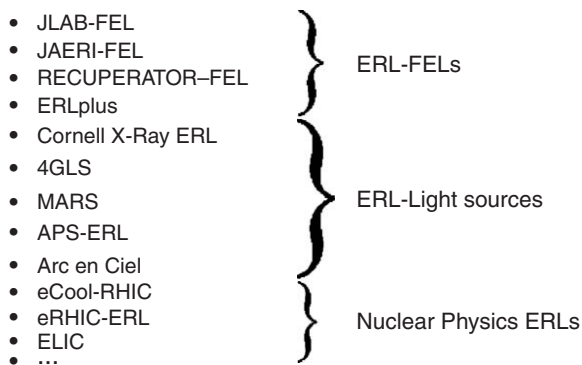


Fig. 1. Illustration of some of the ongoing ERL-based projects.

is a novel next-generation proposal for a UK national light source to be sited at Daresbury Laboratory [1], based on a superconducting ERL with both high average current photon sources (undulators and bending magnets) and high peak current free-electron lasers (FELs). Key features are a high gain, seeded FEL amplifier to generate XUV radiation and the prospect of advanced research arising from unique combinations of sources with femtosecond pulse structure. This suite of sources must cover the whole range from THz to soft X-ray output and be synchronized for pump-probe and dynamic imaging studies.

The project team is now undertaking design studies and this section outlines some of the optics issues addressed by the initial scoping design work and indicates examples where further studies are required to refine and conclude the conceptual design process. The target is to produce a mature proposal by March 2006, including a CDR, to support a funding bid.

From its original concept at Daresbury [2–4], the linac-based source has been considerably developed. Currently, the optics design for 4GLS is being studied and evolved with an aim to agree and to finalize major key parameters in the near future in order to allow the projected CDR timescale to be met.

## 2.2. Layout of 4GLS

The proposed layout of 4GLS has now progressed from its earlier conceptual level [4] to one that is a realistic scheme that can be simulated and that matches the scientific needs of users. Fig. 2 presents a recent version that contains the essential new features, although arc design has still to be finalized. A 10 MeV superconducting gun injects CW beam into the 590 MeV linac and the 600 MeV output beam at 100 mA traverses the outer path, via various undulator sources and a VUV FEL, before returning for energy recovery in a second pass. In parallel, a beam from a high charge (1 nC) RF gun operating at 1 kHz can be accelerated to 160 MeV and then compressed before entering the high-energy linac; a third harmonic (3 GHz) structure is also inserted at this intermediate energy. The emerging 750 MeV beam is separated from the 600 MeV one by a fixed magnetic chicane and directed

through an alternative arc to a further variable energy linac of final output up to  $\sim 1$  GeV. A seeded XUV FEL is located downstream of this, followed by a long undulator for high-energy spontaneous radiation. The source portfolio is completed by an IRFEL fed from a separate 50 MeV linac that is nevertheless synchronized to the high-energy ones via its photocathode gun. The team is investigating a modified layout including cascaded injection to possibly reduce the recirculated beam dump power by additional recovery. A preliminary review of the issues related to cascaded injection indicates that whilst the dump challenges could be reduced by chicane injection and the BBU limit potentially raised by reducing the energy ratio of the two beams in a single linac, the disruptive effects of space charge on the quality of the injected beam would have to be assessed in detail to ensure that the required beam quality could be maintained in the cascaded geometry.

At this stage, the baseline design assumes that both the inner, high-bunch charge loops and the outer, high average current loops are based on Triple Bend Achromat (TBA) cells. Fig. 3 illustrates the lattice functions through the TBA cell of the  $150^\circ$ , 5 cell outer arc for the high average current loop, optimized for isochronous operation (but it can be operated at different values). For this CW loop, the scheme assumes that control of the longitudinal bunch profile through the undulators can be achieved without the use of a “lumped” compressor. The control of the longitudinal dynamics would be achieved by balancing the linac chirp and the  $R_{56}$  of the TBA cells to progressively develop the bunch profile through the various undulators and ultimately optimizing the profile to ensure efficient lasing in VUV FEL.

For the XUV FEL, a detailed assessment of bunch compression schemes has reached similar conclusions to other projects: that a third harmonic RF system is an essential feature and that probably compression should be performed in two stages. The alternative method of  $T_{566}$  adjustment with sextupoles in the arc is less attractive because of the impact on overall optics, but has not yet been abandoned. Present computations suggest that an accelerated bunch of length initially below about 2 ps and 0.02% uncorrelated energy spread can be compressed to well below 100 fs. Checks, using ELEGANT [5] with arc bending fields in the range 0.5–1.0 T reveal CSR energy loss below 0.1% and no significant CSR micro-bunching problems up to 1 nC charge levels. For the low-charge CW branch of 4GLS, increased pre-compression bunch length and energy spread can be tolerated since post-compression energy spread has less importance than for the XUV FEL. However, an upper limit of 7 ps should not be exceeded to avoid severe beam transport non-linearities.

## 2.3. Linac issues

It is our intention to accelerate the CW stream of 80 pC bunches (separated by the RF spacing of 1.3 GHz) from 10 to 600 MeV and every ms to accelerate a 1 nC bunch for the



as part of full Start-to-End simulations which will include the modeling of the FELs within the design. The studies of these issues will allow the baseline layout to be developed into a feasible, conceptual design for the facility by Early 2006.

### 3. Optics issues for the energy recovery linac prototype (ERLP) at Daresbury Laboratory

#### 3.1. Introduction

The second project covered in this paper is the energy recovery linac prototype (ERLP), currently being built at Daresbury Laboratory. This is an accelerator that will serve as a research and development facility for the study of beam dynamics issues and accelerator technology important to the design and construction of the 4GLS facility. Two major objectives of the ERLP are the demonstration of energy recovery and of energy recovery from a beam disrupted by an FEL interaction as supplied by an infrared oscillator system.

#### 3.2. Injector

The injector consists of a high average current DC photocathode gun, a booster and a transfer line to the main linac. The DC photocathode gun is a replica of the 500 kV Jefferson Lab gun [6] and will operate at a nominal accelerating voltage of 350 kV and bunch charge of 80 pC. Electrons will be generated at a GaAs photocathode by the frequency-doubled light (532 nm) of a mode-locked Nd:YVO<sub>4</sub> laser with an oscillator frequency of 81.25 MHz. Two solenoids are used for transverse focusing and emittance compensation, and a normal-conducting single-cell buncher cavity is utilized to decrease the bunch length from the GaAs cathode. The buncher cavity will be operated at 1.3 GHz and is based on the design employed at the ELBE facility. Electrons are accelerated to an energy of 8.35 MeV in the booster, which consists of two superconducting 9-cell TESLA-type cavities operated at 1.3 GHz; the cryomodule design is based on the design of the ELBE linac [7]. The layout of the ERLP injector is shown in Fig. 5 and a description of the design can be found in Ref. [8].

#### 3.3. Space charge in the injector line

A full GPT [9] simulation of the injector line including dipoles and space charge is shown in Fig. 6, a comparison with ASTRA [10] is of course not possible as it cannot model dipoles at present. However, we may compare the results given by GPT together with those using the Vinokurov approximation [11,12], and this is shown in Fig. 6. Spikes in the emittance within the dipole magnets are artifacts arising from the way GPT calculates emittances in a curving trajectory: these should be disregarded. There is a remarkably good agreement between the emittance growth estimated analytically and the one modeled in GPT, except at the exit of

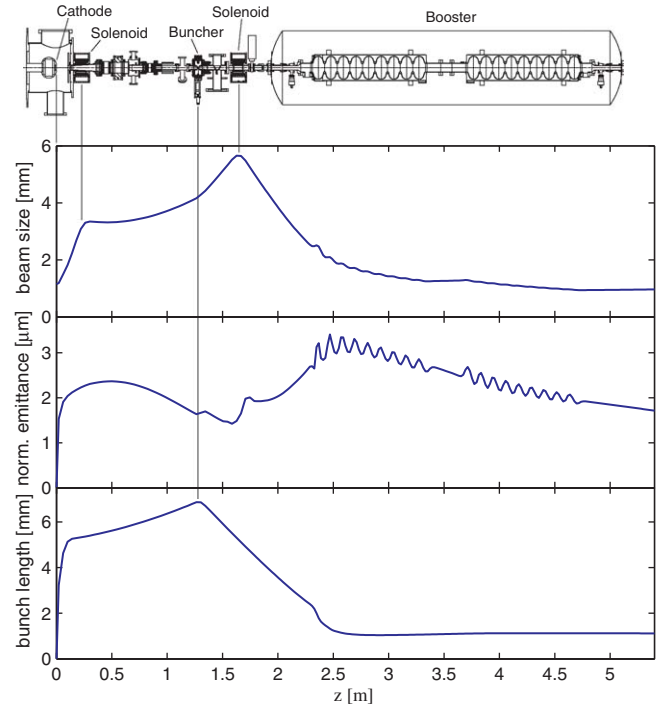


Fig. 5. Layout of the ERLP injector and evolution of the beam size, norm. emittance and bunch length (all RMS).

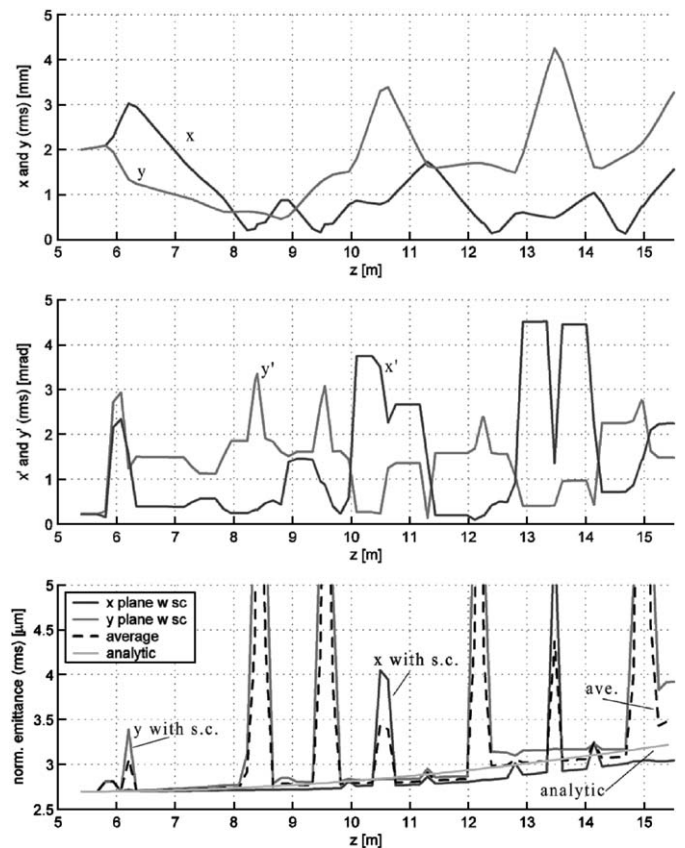


Fig. 6. Transverse beam sizes, divergences and normalized emittance for a Gaussian distribution with space charge for GPT, together with the analytic estimate, for the injector model including dipoles.

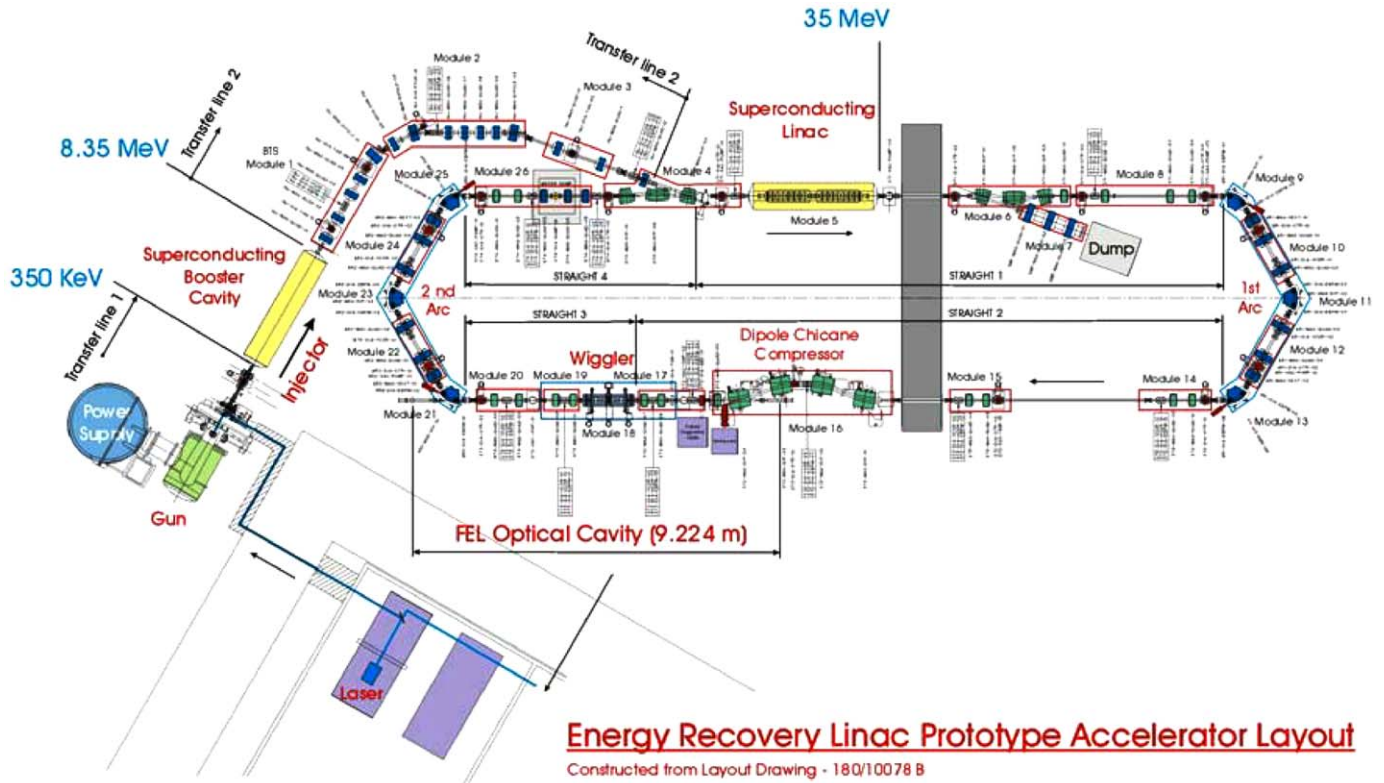


Fig. 7. Present layout of the ERLP.

the last dipole. The reason for the disparity in the last dipole is not yet understood.

### 3.4. Beam transport system

Electrons from the injector are accelerated to 35 MeV in the superconducting main linac, which is identical to the booster and composed of two 9-cell TESLA-type cavities. Two  $180^\circ$  TBA arcs are used to recirculate the beam to the main linac where the electrons are decelerated to their injection energy and subsequently dumped. A 4-dipole chicane provides bunch compression upstream of the wiggler and bypasses the upstream FEL mirror, see Fig. 7.

The minimum bunch length is required within the wiggler. The compression chicane has a static  $R_{56}^C$  of 0.28 m, which requires an off-crest phase of about  $\varphi_{RF} = 9^\circ$  in the main linac for full compression. The TBA arcs are able to provide a variable large negative  $R_{56}$ . In the nominal setup the first arc is set to  $R_{56}^{A1} = 0$  whilst the second is tuned to  $R_{56}^{A2} = -R_{56}^C$  to decompress the bunch. The sextupoles in the first arc can be used to linearize the lowest-order curvature induced by the sinusoidal RF during acceleration, by varying  $T_{566}$ . The sextupoles in the second arc may be used to minimize the energy spread after deceleration for optimal energy recovery and extraction to the beam dump. Preliminary calculations of resistive-wall and bellows wakefield effects indicate that the induced energy spread from these impedances is small. The  $\beta$  functions for the entire lattice of the ERLP are shown in Fig. 8, together with a close up of the waist through the

wiggler in Fig. 9, and the behavior of dispersion in Fig. 10 below.

### 3.5. FEL

The wiggler has been supplied on loan from Jefferson Laboratory, and is a planar device with 40 periods of length 27 mm. The magnet arrays are vertically aligned, focusing in the horizontal plane. The matched beam conditions in transverse phase space are thus a waist in the horizontal plane at the wiggler entrance and a waist in the vertical plane at the wiggler center. This corresponds to a desired  $\beta_x$  at the wiggler entrance of 0.5 m, and  $\alpha_y = 1.75$  and  $\beta_y = 1.25$  m in the vertical plane to give the minimal vertical beam radius averaged along the wiggler.

The optical cavity length is  $D = 9.224$  m with the wiggler positioned at the cavity center; the mirror radii of curvature  $R_1$  and  $R_2$  are chosen to give a near-concentric cavity with an optical waist at the wiggler center. The Rayleigh length is 0.75 m compared to a wiggler length of 1.08 m—the optimum Rayleigh length for FEL coupling would be less than this but would drive the cavity towards instability; the cavity stability is given by  $g_1 g_2 = 0.9$ , with  $g_1 = 1 - D/R_1$  and  $g_2 = 1 - D/R_2$ .

### 3.6. Start-to-End Simulations

The beam dynamics in the high-brightness injector has been modeled including space charge effects using the two

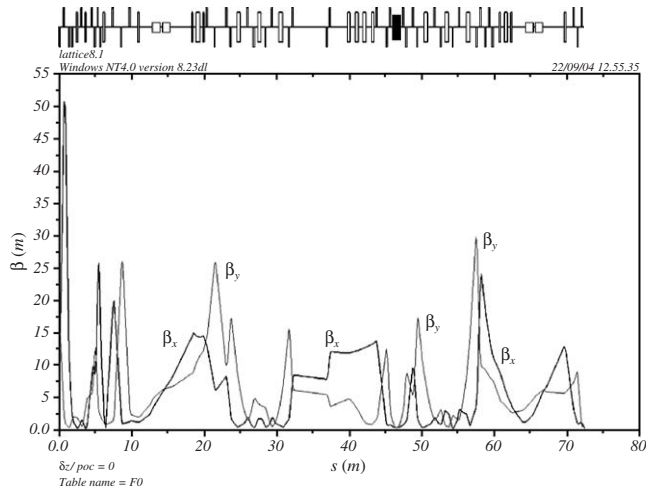


Fig. 8. Beta functions for the ERLP.

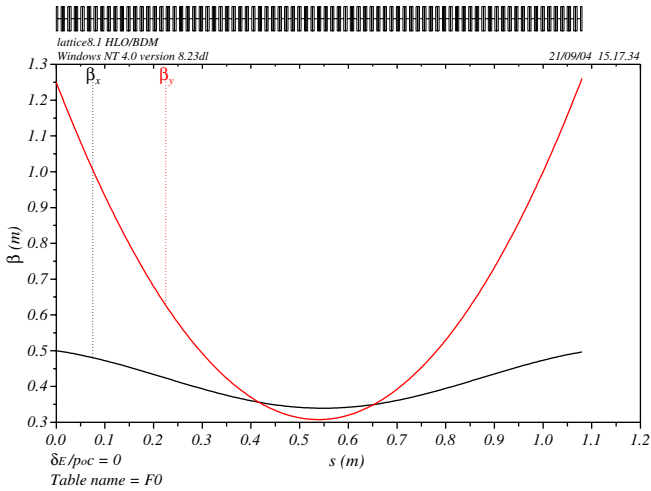


Fig. 9. Close up of beta functions through the wiggler for the ERLP.

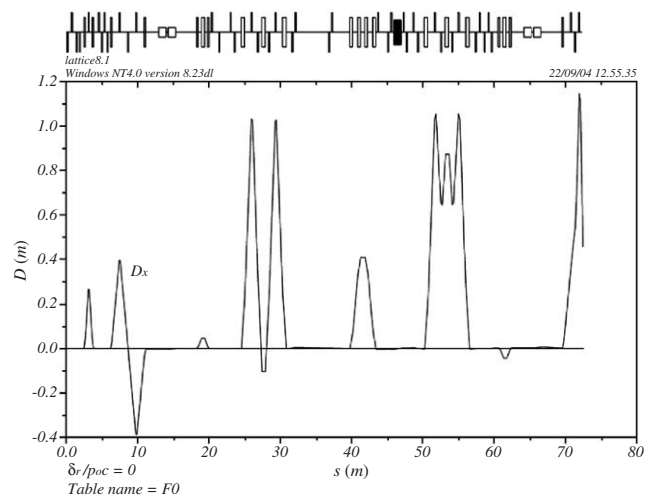


Fig. 10. Dispersion for the ERLP.

codes GPT and ASTRA as described in Section 3.3. The full beamline simulations used the ASTRA code. After the booster, around the arcs the particles have been tracked with the code ELEGANT [5]. The output was examined for any signs of damaging CSR effects but as expected for ERLP this is not a significant issue. The 3D code GENESIS 1.3 was used to model the FEL interaction with the electron beam at 35 MeV.

The performance of an FEL depends crucially on the electron beam parameters. While analytical calculations can give an estimate of the expected performance, the numerical Start-to-End simulations were required to account for various aspects of beam dynamics during the generation, transport and compression of the beam. These studies allowed realistic estimates to be made of the likely large energy spread induced by the FEL process. This was crucial to determine the specification of suitable optics which would allow this disrupted beam to be recirculated for deceleration and then transported into the beam dump [13].

### 3.7. Outlook

The ERLP design has with a relatively straightforward optics design provided a flexible optics which will give the Daresbury physicist a valuable platform to study the range of beam dynamics issues which are of high importance to optimization of the design for the more complex 4GLS project. These studies will take place during the commissioning and optimization period in late 2006 and 2007.

## 4. The Cornell X-ray ERL project

### 4.1. Introduction

This section presents the final light source project overviewed in this paper, and illustrates how the optics issues have influenced the design of an advanced X-ray source based on a relatively high energy ERL. Cornell University has proposed an ERL-based synchrotron-light facility which can provide greatly improved X-ray beams due to the high electron-beam quality that is available from a linac. To provide beam currents competitive with ring-based light sources, the linac must operate with energy recovery, the feasibility of which we plan to demonstrate in a downscaled prototype ERL. Here we present two of several 5 GeV ERL upgrade possibilities for the existing second-generation light source CHESS at CESR. This proposed upgrade suggests how existing storage rings can be extended to ERL light sources with much improved beam qualities. Since today's ring-based light sources have beam energies of several GeV and beam currents a sizable fraction of an Ampere, Cornell is planning a facility that can deliver 5 GeV beams of 100 mA. Continuous beams of these currents and energies would require klystrons delivering a power of the order of a GW to the beam.

Without recovering this energy after the beam has been used, such a linac is impractical.

DC photo-emission sources with negative electron affinity cathodes have been simulated to give less than  $0.4\pi$  mm mrad for a 100 mA beam current in a continuous beam at 1.3 GHz [14]. However, the large beam powers and small transverse and longitudinal emittances required for an X-ray ERL have not been achieved anywhere. CESR has been used for the high-energy physics experiment CLEO and as the 5 GeV second-generation light source CHESS since its construction and it will be available for X-ray physics alone when CESR stops high-energy physics operation. Then we plan to upgrade CHESS to an ERL facility based on the CESR complex.

Cornell University is currently prototyping a DC photoemission electron source and a 10 MeV injector linac [15] for low-emittance beams of high CW currents [16]. The bunches that this injector is designed to produce [17] could be accelerated in the planned X-ray ERL. An X-ray ERL will enlarge the wide range of applications of third-generation light sources by producing beams similar to their CW beams, albeit with much higher brilliance due to the much smaller horizontal emittance and possibly smaller energy spread. At the same time, it can serve more specialized experiments that require ultra-small emittances for high spatial resolution or ultra-short bunches for high temporal resolution [18]. Three different operation modes are planned, one for high flux, one for high brilliance, and one for short bunches. Parameters for these operating modes, not containing the smallest simulated emittances, are shown in Table 1.

The design of the Cornell X-ray ERL should be made cost efficient by reusing much of CESR's infrastructure. The operation of CHESS should be disrupted as little as possible while building and commissioning the ERL, the facility should provide space for a sufficient number of X-ray beamlines. While it could have turned out that reusing CESR imposes too many constraints, quite contrary it has been found that the flexibility of CESR's magnet arrangement holds several advantages for an ERL design. First- and second-order electron optics have been found for bunch compression down to at least 100 fs, and nearly all required magnet strength could be supported by the magnets that are in CESR today. In order to extend the space for cavities, to make space for possible upgrades, and to minimize the impact on CHESS operation, work has been invested in the layout of Fig. 11. It shows the CESR tunnel and the layout of a possible linear ERL extension. Electrons from a 10 MeV injector (1) would be accelerated to the right in a 2.5 GeV linac (2). A return loop (3) would send them into a second linac which is located in the same straight tunnel (4) and accelerates to 5 GeV. An arc (5) injects the electrons into the CESR ring (6) where they travel counterclockwise until another arc (7) injects them back into the first linac, where they are decelerated to 2.5 GeV. The return loop leads the electrons to the second linac section where deceleration is back to 10 MeV and

Table 1

Parameters for an ERL at Cornell University for three different running modes: for high flux, for high coherence and for short pulses

Current (mA)	100	10	1
Charge/b (nC)	0.08	0.008	1.0
$\epsilon_{x/y}$ (nm)	0.1	0.015	1
Energy (GeV)	5.3	5.3	5.3
Rep. rate (GHz)	1.3	1.3	0.001
Av. flux (ph/0.1% s)	$9 \times 10^{15}$	$9 \times 10^{14}$	$9 \times 10^{12}$
Av. brilliance (ph/0.1% s mm <sup>2</sup> mrad <sup>2</sup> )	$1.6 \times 10^{22}$	$3.0 \times 10^{22}$	$2.0 \times 10^{17}$
Bunch length (ps)	2	2	0.1

We show initial target emittance figures, simulations suggest that lower values may be possible.

leads to the beam dump (8). The South half of the CESR tunnel would contain undulators and would reuse the current facilities of CHESS. Additionally, new user areas could be created in the North section of CESR (at the top of the figure) and in straight sections of the linac tunnel. The location of the linac at a hillside is chosen in such a way that no existing building foundations interfere and that X-ray beamlines with easy access can be added between the linac and CESR.

A return arc is also shown which connects the arcs (5) and (7) so that electrons can return to the linacs after acceleration without passing through CESR. This connection has been chosen so that the ERL could be built and commissioned while CESR is still used as a storage ring light source. Other advantages of this upgrade plan are that all of the CESR tunnel is reused, which creates space for a large number of insertion devices.

To limit the cost of cooling, the accelerating gradient of the SC cavities should not exceed 20 MV/m. Thus, 250 m of cavities would lead to 5 GeV beam energy. However, much more space is required for the linac, since HOM dampers and connecting tubes have to be placed after each cavity and two quadrupoles have to be placed after each cryomodule of ten 7-cell cavities. Our analysis, which is based on the 1.3 GHz cavity cell shape of the TESLA design, on four HOM couplers of the TTF type per cavity, and on one ferrite HOM damper of the CESR type per cavity, showed that for a beam tube radius of 39 mm we could not obtain a fill factor larger than 53%. The total linac length would therefore have to be about 500 m. The tunnel extension shown in Fig. 11 has a section of 250 m with two linacs side by side. A sketch of a possible tunnel cross-section is shown in Fig. 12. A straight tunnel housing two linacs reduces tunnel cost as well as the required length of cryogenic lines and cables. The tunnel is laid out longer than required for the two linacs, so that an extension of the facility by extra undulators or by an FEL is possible.

#### 4.2. Arc optics

We studied whether a favorable optics can be found for the CESR South arc in spite of the constraints imposed by

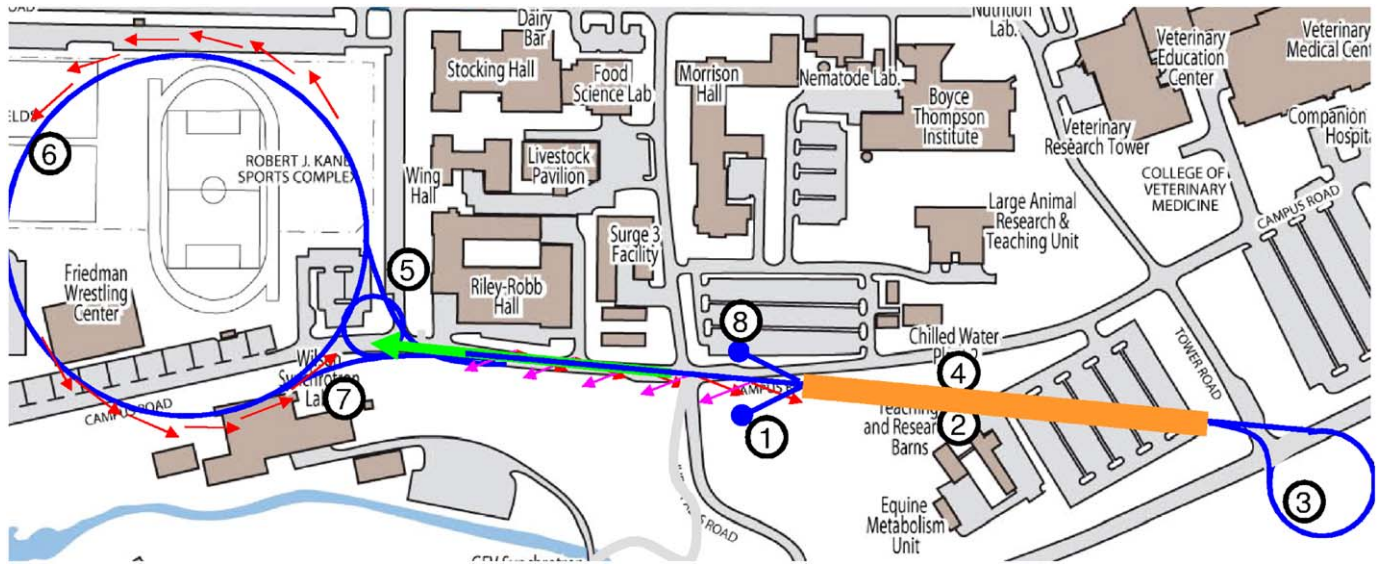


Fig. 11. An ERL in an extended CESR tunnel.

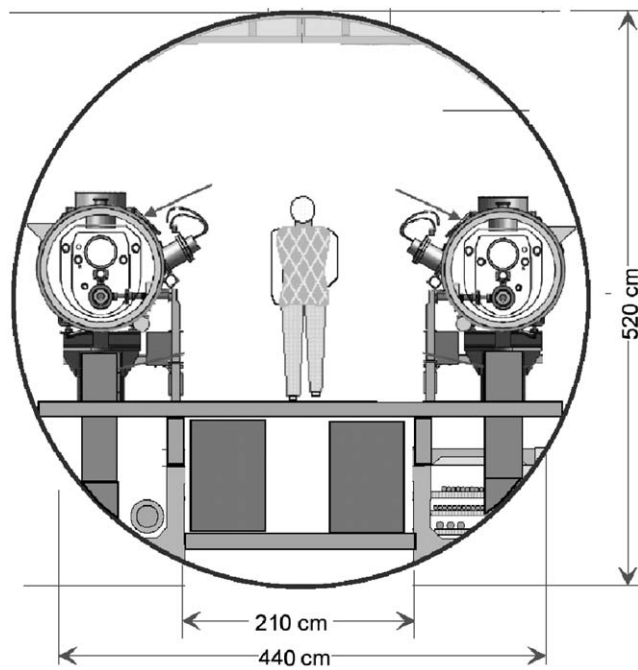


Fig. 12. Sketch of a cross-section of a tunnel with two linacs.

the existing tunnel. To reuse as much as possible from CESR, we maintained the bending magnets and quadrupoles in their current positions and only replaced the regions where the undulators would be installed. Each of 7 undulators has two matching quadrupoles at each side and is separated from the next undulator by a three-bend achromate. Finding an optics for the operation with 2 ps bunch length turned out to be relatively simple. The matching constraint were  $\beta = 1, 2.5, 2.5, 12.5, 2.5, 2.5, 1$  m in the seven successive undulators, and  $\alpha = 0, D = 0, D' = 0$  in these seven places. The optics for an RMS bunch

length of 100 fs has to fulfill several additional requirements. The RF acceleration phase  $\varphi$  and the first- and second-order time of flight terms  $R_{56}$  and  $T_{566}$  of the first half of the arc have to be chosen to yield the desired bunch length in the central undulator [19]. For the second half of the return arc,  $R_{56}$  and  $T_{566}$  are determined by minimizing the energy spread after deceleration. The beta function and the dispersion for the return arc are shown in Fig. 13. Even though the magnet arrangement is symmetric around the center of the arc, the optics functions are not symmetric since the conditions for  $R_{56}$  and  $T_{566}$  are different for the two halves. The second-order time of flight term  $T_{566}$  is influenced by sextupoles and has to have the same sign as  $R_{56}$ . This is hard to achieve in the achromatic arrangements that have been proposed for this purpose. However, with the FODO-like optics of the CESR arc, this can be achieved with relatively weak sextupoles. This advantage is due to the large dispersion after the linac. The nonlinear dynamics in sextupoles can increase the emittance. However, due to the weak sextupoles and the small transverse beam size, the dynamics is so weakly nonlinear that only the second-order dispersion  $T_{166}$  and its slope had to be eliminated in the center of the return arc. The second-order conditions on  $T_{566}, T_{166}$  and  $T_{266}$  were satisfied by three sextupoles on each side of the arc close to the three maxima of the dispersion in Fig. 13. For short-bunch operation, CSR can also increase the emittance. The emittance growth was computed with the code ELEGANT and is shown in Fig. 14. Since the beam dilution due to the nonlinear dispersion is included, the emittance is shown to decrease where the second-order dispersion is corrected. In the central undulator, the emittance for 100 fs bunch length has only increased by a factor of 1.8. To limit the emittance growth, it was found prohibitive to compress the bunch length to its minimum since this creates a spike in the longitudinal density and strongly enhances CSR. We

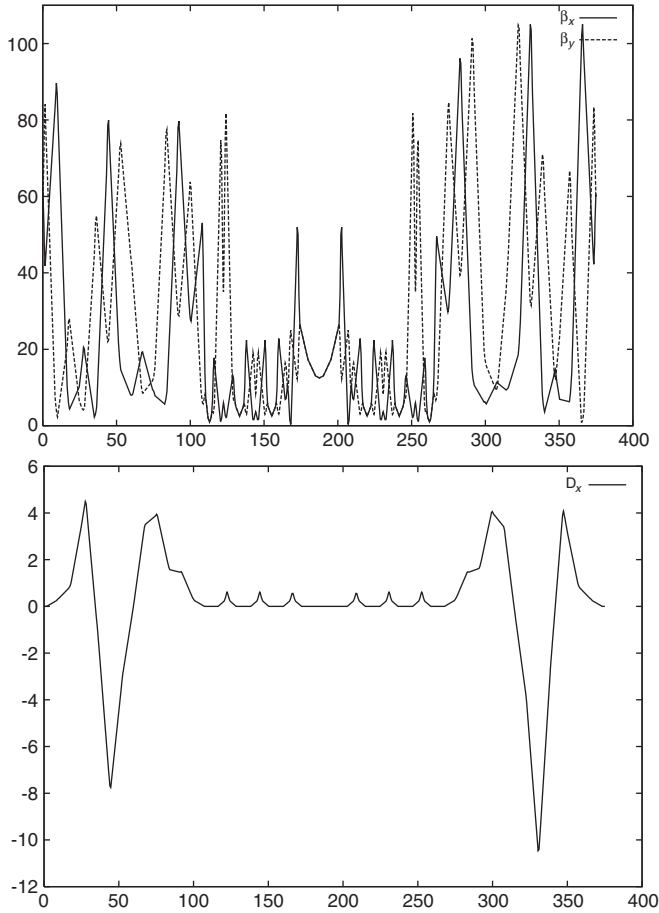


Fig. 13. Beta functions and dispersion in the arcs. Units are meters.

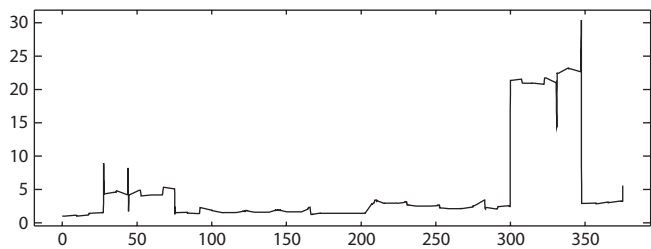


Fig. 14. Effective normalized horizontal emittance along the arc. Units are micro meters.

therefore increased  $\varphi$  to obtain 100 fs bunches without full compression.

To the seven undulators in the South section and the seven in the North section of CESR, additional undulators could be placed in the section between the linac and CESR, which has been designed with a gentle arc of achromats.

#### 4.2.1. Two linacs and return loop

The loop (3) connecting the two linacs was chosen so as to produce an acceptable emittance increase due to synchrotron radiation. Fig. 15 shows an optics with 16 achromatic cells. The magnet in the center of each cell has a negative bend to make the lattice isochronous, it has a

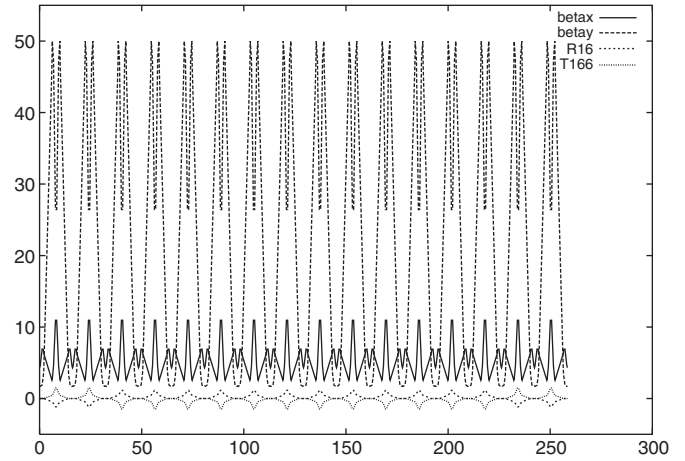


Fig. 15. Optics of the return loop. Units are meters.

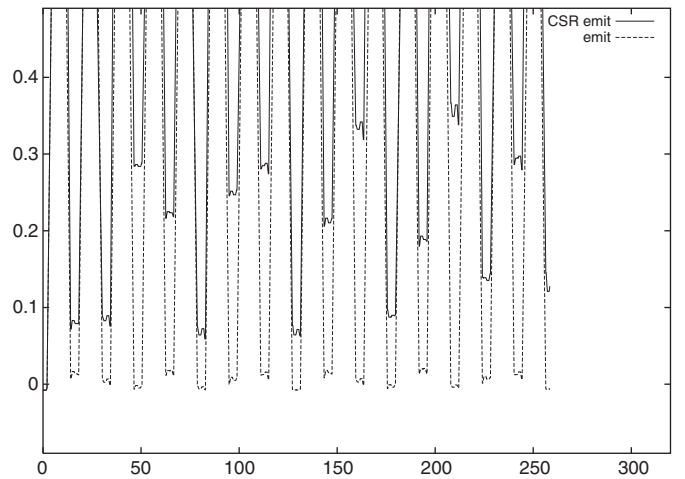


Fig. 16. CSR emittance growth in the return loop. Solid: with CSR, dashed: without radiation. Units are % of 0.1 nm along the linac (in m).

horizontally focusing quadrupole which produces a very small average horizontal beta function, and it has a sextupole to correct the second-order dispersion. After this correction, nonlinear dynamics does not lead to emittance growth for a 0.2% energy spread beam that one obtains for  $6^\circ$  off-crest acceleration, as required for compressing a 2 ps long bunch to 100 fs after the linac. This loop could also be used for energy spread reduction by running the second linac  $-6^\circ$  off-crest as discussed in Ref. [19].

The emittance growth for a 100 mA beam due to incoherent synchrotron radiation for the high-flux option in Table 1 is 0.04 nm and therefore acceptable. The emittance growth due to CSR as computed by ELEGANT [5] is shown in Fig. 16. The fluctuations are due to second-order dispersion, but the difference between the two curves shows the influence of CSR. It is approximately 0.006 nm and thus negligible.

The optics for the linear accelerator is shown in Fig. 17 in  $x$  and  $y$  for the accelerating beam. Both linacs are

shown, but the optics of the return loop is not shown in between them. The optics for the accelerating beam is shown, that for the decelerating beam of the ERL is mirror symmetric. The beta functions are relatively small. The threshold current of the BBU instability has been

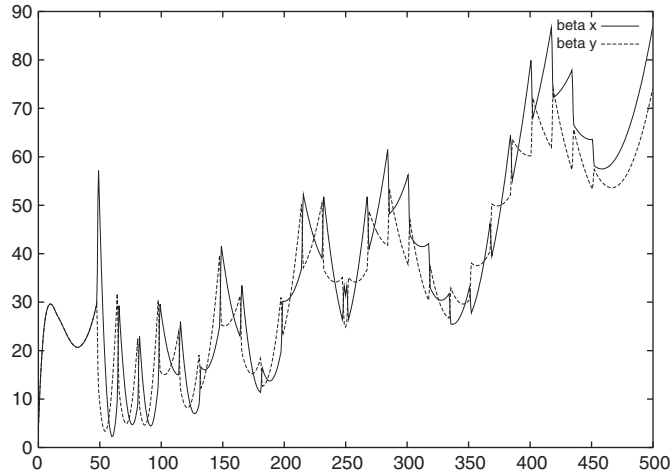


Fig. 17. Optics in the two linacs (units are m).

calculated for a similar optics [20]. For quite pessimistic assumptions (HOMs with  $R/Q$  of  $100 \Omega$  and  $Q = 10^4$ ) the threshold current is about 200 mA for a HOM frequency randomization of 1.3 MHz. When the modes are polarized and an optics is chosen that couples horizontal oscillations to the vertical and vice versa [21], the threshold current is about 650 mA.

Emittance growth due to CSR is a phenomenon which is hard to compute accurately. We are therefore also investigating alternate designs which minimize the total bend angle of the ERL similar to what was presented in Ref. [22]. A possible layout that is adjusted to the geography of the Cornell campus is shown in Fig. 18.

### 4.3. Beamlines

The South half of the CESR tunnel would contain undulators and would reuse the current facilities of CHSS. Additionally, new user areas could be created in the North section of CESR (at the top of Fig. 11) and in straight sections of the linac tunnel. The location of the linac at a hillside is chosen in such a way that no existing building foundations interfere and that X-ray beamlines

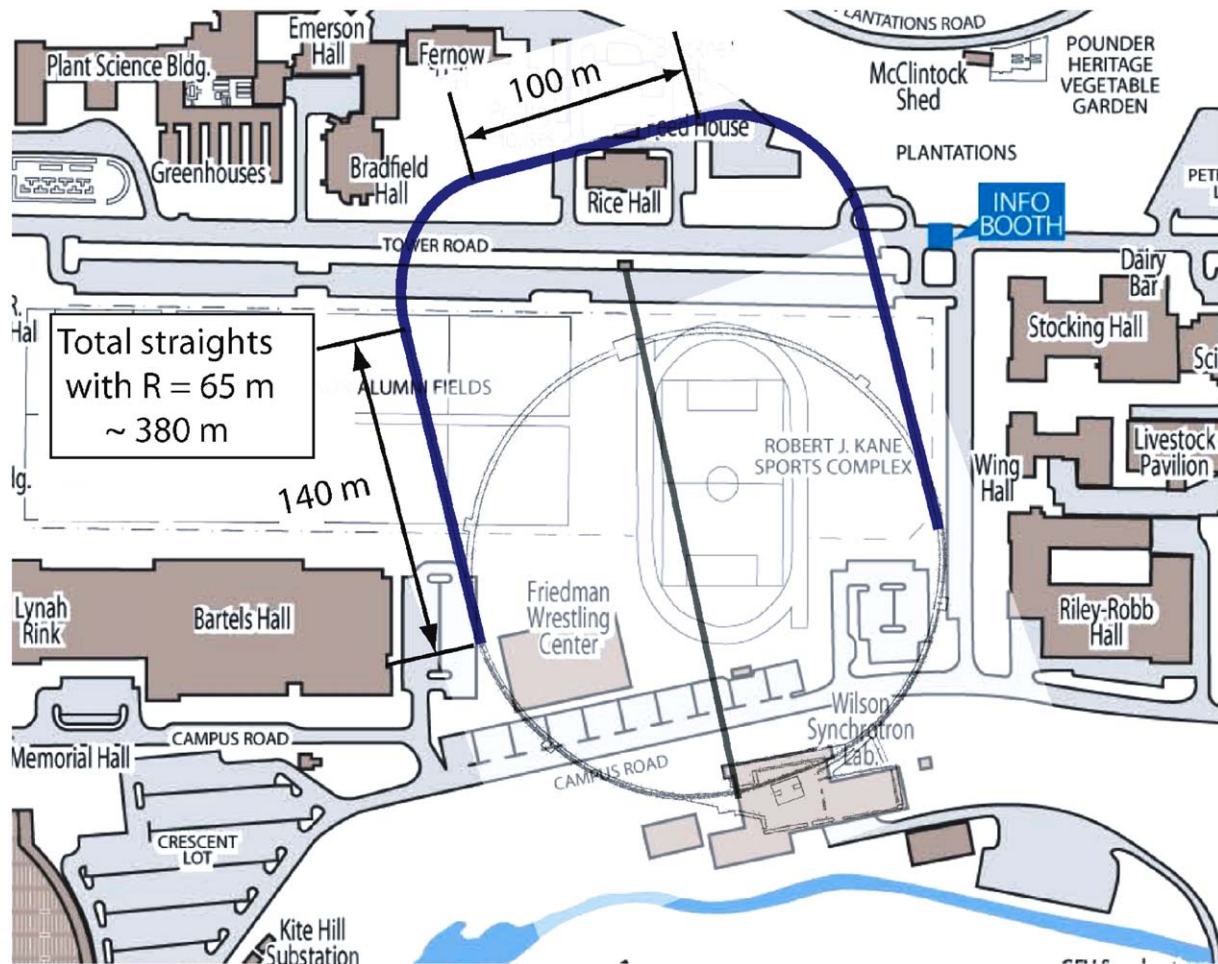


Fig. 18. An ERL in the extended CESR tunnel minimizing bend angles.

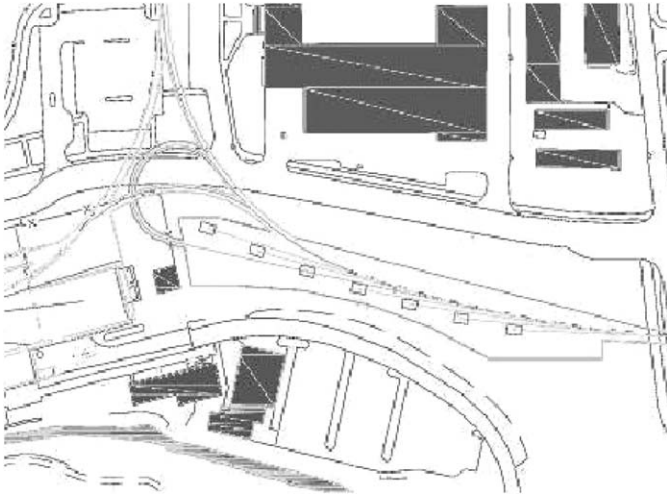


Fig. 19. The beamline connecting the linac and the CESR ring. Undulator beam lines are shown, but a CW FEL could also operate in this region.

with easy access can be added between the linac and CESR. The outline and the optics for this section is shown in Figs. 19 and 20. The presented optics of Fig. 13 modifies CESR as little as possible. It contains four undulators of 5 m length, two undulators of 2 m length and one 25 m long undulator in the South, and an equivalent arrangement could be added in the North. The beta functions are 1, 2.5 and 12.5 m in the center of these undulators, respectively, but a flexible lattice can produce larger beta functions easily. Currently, 18 beamlines and their science case are being investigated. The undulator lengths are: 25 m for 2, 5 m for 9, 2 m for 2, 1 m for 1, 2 m for 3 undulators in the 2.5 GeV loop in the East, and one diagnostic undulator. These studies cover the areas of: phase imaging and topography, coherent diffraction and XPCS microscopy on the nm scale, nanoscope and nanoprobe TXM and STXM to nm resolution, protein crystallography, inelastic X-ray scattering, femtosecond timing, resonant scattering, SAX and XPCS for mesoscopic science, and general material science, e.g. at high pressures. The undulators at 2.5 GeV would be for soft X-ray studies.

#### 4.4. Optics

The loop (3) connecting the two linacs was chosen so as to produce an acceptable emittance increase due to synchrotron radiation. After appropriate nonlinear correction, the dynamics does not lead to emittance growth for a 0.2% energy spread beam that one obtains for 6° off-crest acceleration, as required for compressing a 2 ps long bunch to 100 fs after the linac. This loop could also be used for energy spread reduction by running the second linac –6° off-crest as discussed in Ref. [19].

#### 4.5. Summary

By addressing the major optic issues at the design stage, it has been shown that an extremely advanced light source

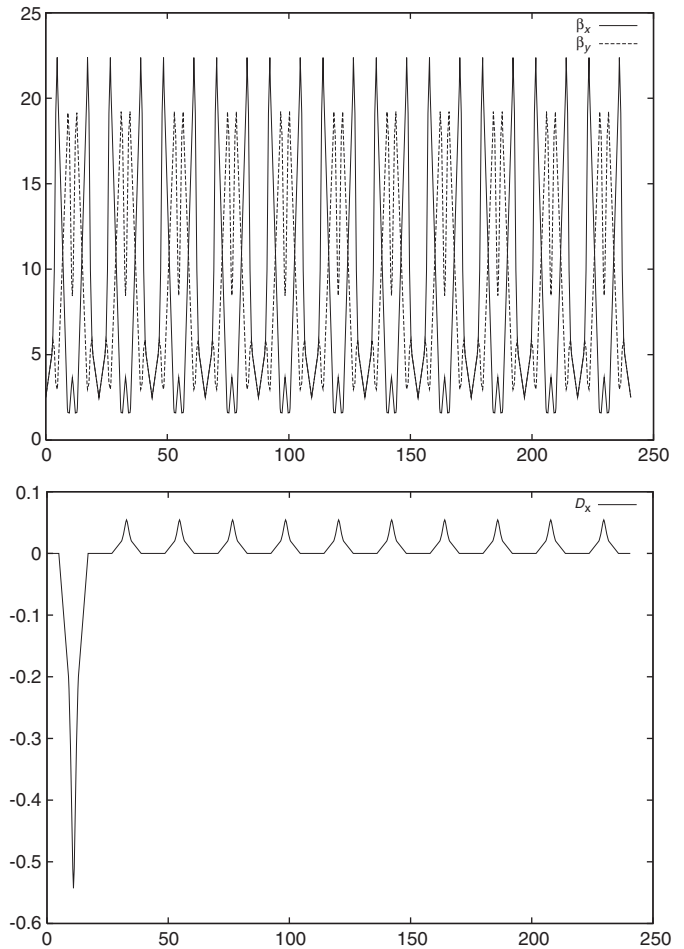


Fig. 20. Beta functions and dispersion for the region between the linac and CESR (units are in m).

can be designed on the Cornell site which would provide a very high quality and versatile range of X-ray sources from a number of undulators.

### 5. Optics issues for ERL projects at BNL

#### 5.1. Introduction

Looking at the proposed ERL-based accelerators at the Brookhaven National Laboratory provides an opportunity to consider ERL optics issues from the perspectives of designer whose primary aims is to produce beams satisfying the challenging demands of the high-energy and nuclear physics communities. The Collider-Accelerator Department (C-AD) at Brookhaven National Laboratory is pursuing development of ERL-based accelerators for multiple applications in high energy and nuclear physics [23]. These programs are aimed towards a ten-fold increase in the heavy ion luminosity at the Relativistic Heavy Ion Collider (RHIC) [24,25] and development of an ERL-based electron-ion collider, known as eRHIC [26]. As part of this program, we are designing, constructing and commissioning a dedicated ERL for R&D studies of issues relevant to

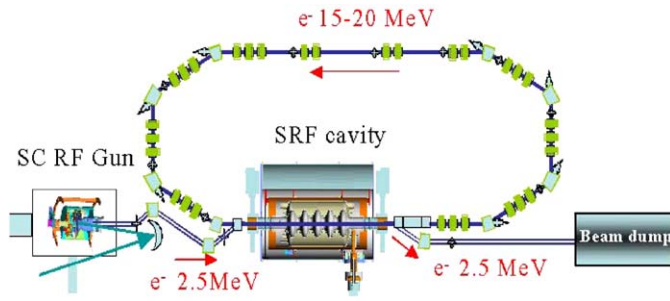


Fig. 21. Layout of the R&D ERL.

Table 2  
Electron beam parameters of R&D ERL

Mode of operation	High bunch charge	High current
Initial bunch length (ps)	70	45
Initial beam radius (mm)	4.0	2.5
Field on the cathode (MeV/m)	44.2	27.8
Injection energy (MeV)	3.7	2.5
Maximum beam energy (MeV)	21	20
Average beam current (A)	0.2	0.5
Bunch rep-rate (MHz)	10	350
Charge per bunch (nC)	10	1.4
<b>@2.5 MeV</b>		
Normalized emittances (x/y), mm mrad	13.4/9.2	4.1/4.1
Longitudinal emittance (with/without third harmonic RF), ps keV	62/240	19/58
<b>@20 MeV</b>		
Normalized emittances (x/y), mm mrad	14.5/7.8	2.5/1.3
Longitudinal projected <sup>a</sup> emittance (with/without third harmonic RF), ps keV	183/1140	42/700

<sup>a</sup>Note: real value of the longitudinal emittance remains very small while RMS value is determined by the curvature of the accelerating field.

operating with high-current, high-brightness electron beams [27]. All three ERLs at BNL will be based on superconducting RF cavities (guns, linacs, etc.) operating at a frequency of 703.75 MHz [23].

### 5.2. Optics issues of BNL’s R&D ERL

The R&D ERL facility at BNL, shown schematically in Fig. 21, aims to demonstrate CW operation of an ERL with average beam current in the range of 0.1–1 A, combined with very high efficiency of energy recovery. Projected parameters of this ERL are summarized in Table 2. Electrons are generated and accelerated in a superconducting half-cell gun to about 2.5–3.5 MeV. They are injected into the ERL loop through a zigzag merging system, a novel dispersion-free merger for space charge dominated beams incorporating an emittance compensa-

tion scheme (see Ref. [28] in this issue). Two solenoids are used for transverse focusing in the injection system. An SRF 5-cell linac [23,29] accelerates electrons up to 20 MeV, and the accelerated electron beam passes through a return loop comprised of two achromatic arcs with a straight section between them before returning to the same linac. The path length of the loop provides for 180° change of the RF phase, causing electron deceleration in the linac (hence the energy recovery) down to 2.5 MeV. The decelerated beam is separated from the higher-energy beam and is directed to the beam dump.

The flexible lattice of the ERL, shown in Fig. 22 has 30 individually controlled quadrupoles and provides for independent control of the most important elements of the transport matrix:

$$\begin{bmatrix} x \\ x' \\ y \\ y' \\ -c\delta t \\ \frac{\delta E}{E} \end{bmatrix}_{s_2} = \begin{bmatrix} R_{11} & R_{12} & \dots & \dots & \dots & D_x \\ R_{21} & R_{22} & \dots & \dots & \dots & D'_x \\ \dots & \dots & R_{33} & R_{34} & \dots & D_y \\ \dots & \dots & R_{43} & R_{44} & \dots & D'_y \\ \dots & \dots & \dots & \dots & R_{55} & R_{56} \\ \dots & \dots & \dots & \dots & \dots & R_{66} \end{bmatrix} \times \begin{bmatrix} x \\ x' \\ y \\ y' \\ -c\delta t \\ \frac{\delta E}{E} \end{bmatrix}_{s_1}$$

The adjustable part of the lattice has two arcs and a straight section. Each arc consists of the two 60° chevron dipoles, two 30° dipoles with parallel edges, and three quadrupole triplets. A bending radius of 20 cm was chosen for the dipoles to provide a possibility of using the visible part of synchrotron radiation spectrum from a 20 MeV electron beam for beam diagnostics. The chevron 60° dipoles split the focusing between vertical and horizontal directions in the dipoles. The quadrupole triplets between the dipoles allow us to control the value and the sign of longitudinal dispersion, while keeping the arcs achromatic. Eight quadrupoles in the dispersion-free straight section provide for matching of the β-function and for choosing the desirable phase advances independently in the horizontal and vertical planes. The lattice has complete independent control of these values and the signs of matrix elements  $R_{12}$  and  $R_{34}$ , which are critical for transverse stability, and  $R_{56}$ , which is critical for longitudinal stability of the beam. The optics functions for one turn for the case of  $R_{56} = 0$  is shown in Fig. 23. The loop has a full assortment of horizontal and vertical correctors and beam position monitors. The ERL has been under construction since 2004 and commissioning is planned in 2007. This

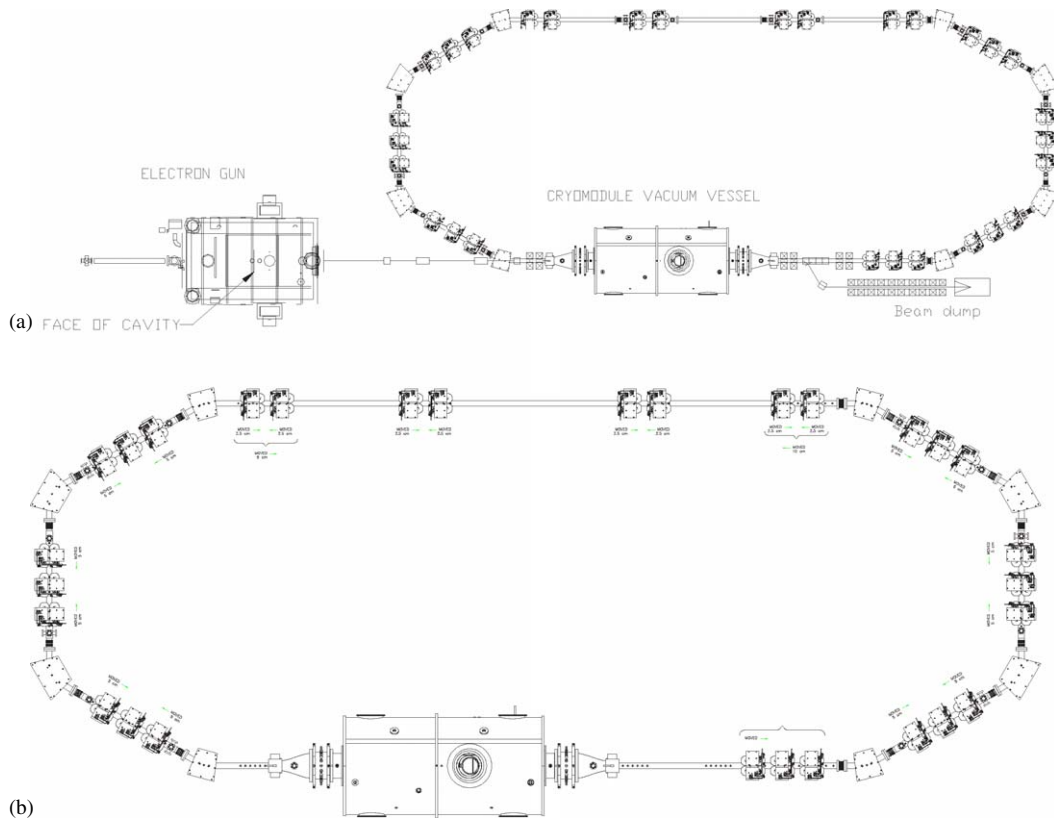


Fig. 22. Drawing of the R&D ERL loop.

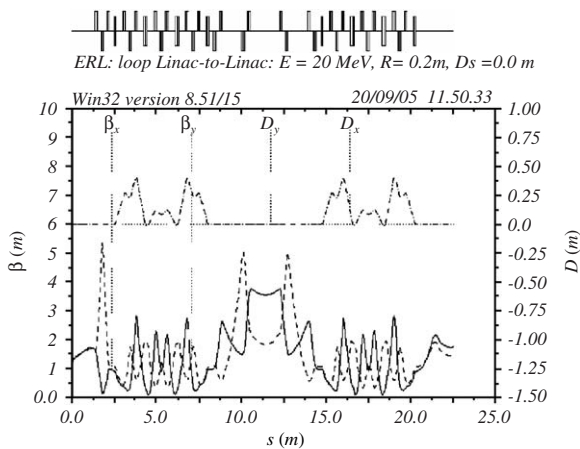


Fig. 23. Lattice  $\beta$  and  $D$  functions of the R&D ERL for the case of zero longitudinal dispersion  $D_s = R_{56}$ .

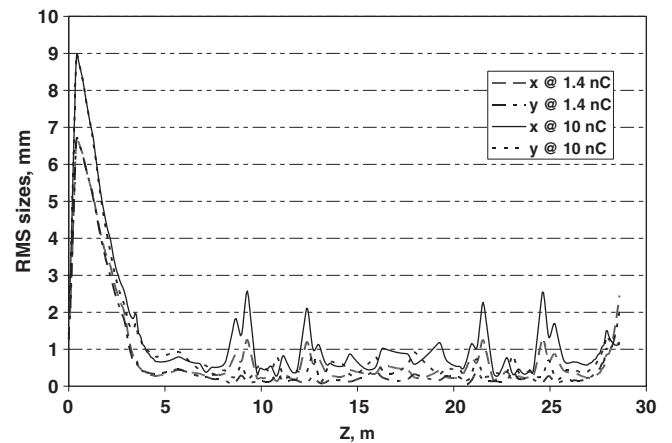


Fig. 24. Evolution of the RMS beam sizes in the R&D ERL with charges of 1.4 and 10 nC per bunch.

ERL will serve as a test bed for testing the limits of transverse and longitudinal stabilities of intense ampere-class CW electron beams.

Space charge effects play a very significant role in the R&D ERL and require careful Start-to-End simulations. Beam-size envelopes for 1.4 and 10 nC electron bunches starting from the photocathode to the exit from the ERL were obtained with PARMELA [30], and are shown in Fig. 24. The remaining R&D ERL beam parameters are summarized in Table 2.

### 5.3. Optics issues of e-Cooler ERL

The RHIC electron cooler, currently in an R&D phase, requires a 54 MeV electron beam, which cannot be produced by an electrostatic accelerator. R&D of electron beam cooling in RHIC [31] leads to the following electron beam parameters: energy of 54 MeV, bunch charge of 20 nC, bunch repetition frequency of 9.4 MHz, energy spread of the order of  $10^{-4}$ , RMS normalized emittance better than  $40 \mu\text{m}$ , magnetization of about 2–5 T mm<sup>2</sup>. The parameters

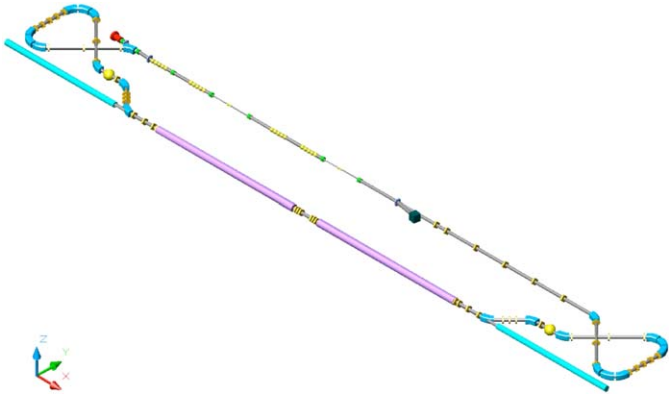


Fig. 25. Layout of the RHIC cooler.

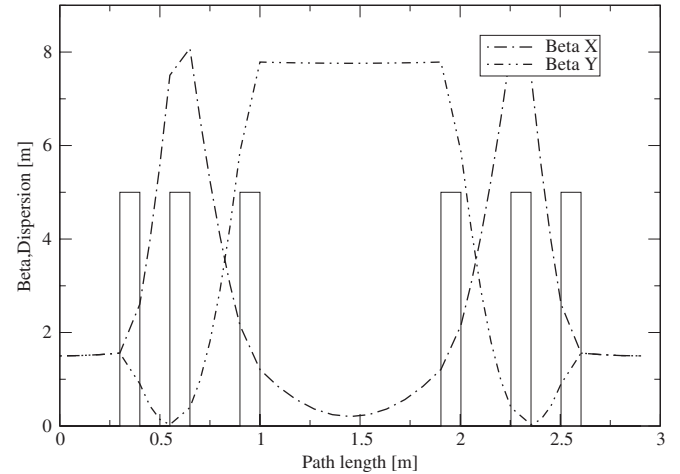


Fig. 26. Optics of the matching section between the cooling solenoids.

of an electron beam required for electron cooling of RHIC are similar to those of the R&D ERL, but the ERL for these systems have some significant differences. The e-cooler ERL [32], shown in Fig. 25, will operate with a magnetized electron beam generated from a cathode submerged in a solenoidal magnetic field. When electrons leave the solenoidal field, the magnetization is transferred into mechanical angular momentum equivalent to a very large correlated emittance when projected onto  $x-x'$  and  $y-y'$  phase space planes. This magnetization, i.e. the correlations, must be preserved through the entire acceleration and transport process to be used in the cooling solenoid. This requirement significantly complicates the ERL lattice.

One present design, shown in Fig. 25, uses flat-to-magnetized beam converters [33] to preserve the quality of the electron beam. A number of cavities operating at the fundamental (703.75 MHz), 3rd harmonic (2.1 GHz) and low frequency (200 MHz) are used to provide matched length and low-energy spread of the electron beam in the cooling section. Two achromatic stretcher loops with a large value of  $R_{56}$  (and two 200 MHz RF cavities) are used to initially increase the bunch length of the electron bunch from a few millimeters to about 30 cm (i.e. the length of ion bunches in RHIC) and to compress it back after it passed the cooling section.

We must also decouple the cooling section for the hadron beam. To accomplish this, the cooling solenoid is split into two equal sections, with opposite field directions, giving a zero net hadron beam coupling. This requires a change in the direction of the electron beam magnetization between the two opposite solenoid sections, which will be achieved [34] using a quadrupole matching section providing a phase advance of  $180^\circ$  and a vertical phase advance of  $360^\circ$ . Fig. 26 shows the optics for this matching section.

#### 5.4. Optics issues of ERL-based eRHIC

The detailed beam parameters and proposed configurations for an ERL-based polarized electron-hadron collider eRHIC are presented in Refs. [23,25]. Table 3 gives a brief

Table 3

Main parameters of electron beam in the eRHIC

Mode of operation	Collider	Light source
Circumference (m)	3834	3834
Beam rep-rate (MHz)	28.15	703.75
Beam energy (GeV)	5–20	5–20
$\gamma$ , Relativistic factor	$1-4 \times 10^4$	$1-4 \times 10^4$
RMS normalized emittance ( $\mu\text{m}$ )	5–50	0.9
Beam emittance @ 20 GeV ( $\text{\AA}$ )	1.25–12.5	0.18
Full transverse coherence at $\lambda$ , ( $\text{\AA}$ )	1.13	11
or at photon energy (keV)		
RMS Bunch length (ps)	30	0.03–3
Charge per bunch (nC)	1.6–16	0.7
Average e-beam current (A)	0.045–0.45	0.5

summary of the electron beam parameters for the collider and light source mode of eRHIC operation. Two of the most attractive features of ERL-based eRHIC are full spin transparency of the ERL at all operational energies and the capability to support up to four interaction points (IPs). Issues related to spin transparency are described in Refs. [23,25].

The parameters of the polarized electron beam are very impressive and this facility could easily be used as a next-generation light source. In addition, RHIC rings operate for only about 30 weeks per year, which leaves about 4 and a half months for dedicated mode of ERL operation as a light source. In this case unpolarized electrons with lower charge per bunch and a higher rep rate will be used, while keeping the same level of average electron beam current ( $\sim 500$  mA). These parameters of the electron beam in eRHIC's ERL naturally match the requirements for a next-generation light source.

The ERL for eRHIC operates on the same principles as the R&D ERL, with some differences: the eRHIC electron gun will generate longitudinally polarized electrons using GaAs photocathode driven by a high-power circularly polarized laser beam from a small-size FEL (also driven by a smaller ERL) [25].

There are two designs of ERL for eRHIC: a 5–10 GeV stand-alone ERL (see Fig. 28) and a 5–20 GeV ERL with the return loops located in the RHIC tunnel (see Fig. 5 in Ref. [23]). Both designs have low- and high-energy loops to separate the function of generating and disposing the electron beam from the main acceleration process. Furthermore, the high energy of electrons in eRHIC causes a significant loss of energy at the MeV scale, which must be compensated by a special RF system.

The stand-alone ERL has four major and two minor arcs, as shown in Fig. 27. It is comprised of a rather simple FODO lattice with high density, but low-field dipoles for reducing synchrotron radiation losses to about 5 MeV for the entire cycle from the gun to the dump. The arc with the largest energy of electrons incorporates the IP. Polarized electrons with initial energy of 5 MeV are injected into the first ERL with a 500-MeV superconducting linac. They pass twice through this linac before entering the main ERL. The main ERL has two linacs with a nominal energy gain of 2250 MeV per linac. Passing twice through each linac, the electron beam reaches a maximum energy of 10 GeV. During the process of acceleration in the ERL, the electron beam passes through the arcs where it loses about 2.5 MeV

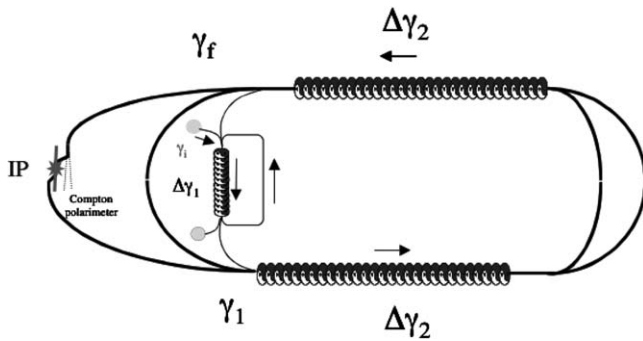


Fig. 27. A standalone ERL for eRHIC.

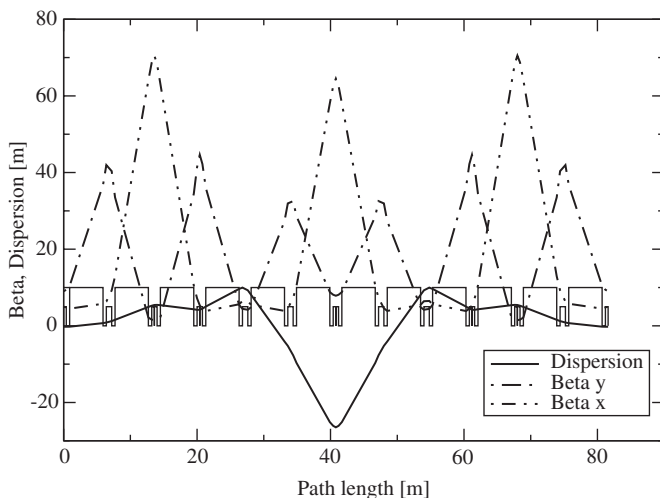


Fig. 28. Lattice of achromatic arc for a stand-alone ERL.

of its energy in the form of synchrotron radiation. At full energy, the electron beam passes through a half arc towards the IP. A Compton laser polarimeter installed in the dogleg just before this acquires final measurements of the electron beam's polarization in the IP. Each normal arc or transfer line of the ERL ensures a delay in electron beam time equal to an integer number of RF cycles. In this case, all linacs will synchronously accelerate (or decelerate) electrons. The last arc with the IP and vertical chicane is a special one—it provides for a delay in the electron beam time equal to an integer number plus a half of RF cycles to change the accelerating sequence into a decelerating one. It also incorporates a special cavity to compensate for the synchrotron radiation loss.

The main ERL-based design of eRHIC is based on the main arcs sharing the 3.8 km circumference RHIC tunnel, Fig. 29. Leveraging the RHIC tunnel for ERL's arcs significantly increases the radii of curvature and reduces synchrotron radiation loss. With 85% filling factor for the arcs, the 10 GeV ERL will have energy loss of less than 2 MeV per pass and very low linear power density of synchrotron radiation of 0.22 kW/m. The linear power density of synchrotron radiation will reach the level of 8.8 kW per meter, presently attained at the B-factory, for a 25 GeV ERL.

On the way to the final energy the electron beam passes through the arcs, where synchrotron radiation may significantly affect the electron beam parameters. Our present design is based on 150 25-m long achromatic cells (see Fig. 3 in Ref. [27]) with a bending radius of 400 m in the dipoles. The total synchrotron radiation energy loss is 35 MeV for 20 GeV electrons. This rather mundane triplet lattice in the main arcs [27] provides for complete preservation of the transverse emittance (to be exact, the horizontal emittance grows for  $1.6 \times 10^{-3}$  nm-mrad for a 20 GeV beam). At the same time, the quantum fluctuations of synchrotron radiation determine the relative energy spreads for both 10 and 20 GeV electron beams, which still remain very low at  $2.5\text{--}5 \times 10^{-5}$  level [27].

Using the ERL with a low-emittance electron beam dramatically simplifies the lattice of the interaction region [25,35]. Single pass interaction of electrons with the ions and very low emittance of the electron beam allows the use of large  $\beta^*$  ( $\sim 1$  m) for the electron beam, while matching the transverse size of electron and hadron beams. Smaller electron beam emittance results in a 10-fold smaller aperture and angular acceptance requirements for the electron beam and permits movement of the focusing quadrupoles for the electron beam outside the detector and the IP region, while leaving the dipoles to separate the beams. Therefore, the electron side of the IP optics does not present significant new challenges.

Collisions with hadrons significantly modify the distribution of the electron beam (see Fig. 30). This requires tuning of the ERL optics during operation depending on the hadron beam intensity. A triplet following the IP can easily accomplish this. The main challenge of the IP design

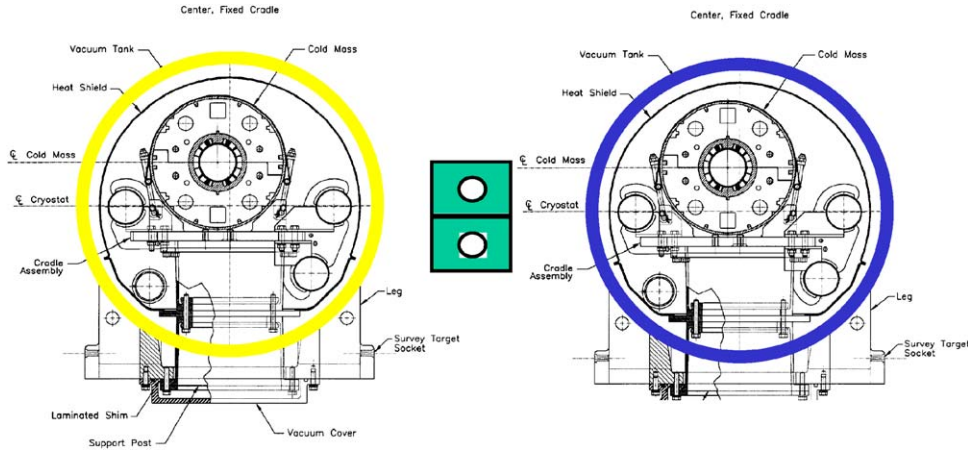


Fig. 29. Schematic of the arcs (rectangles) for the linac-ring eRHIC located in the RHIC tunnel on the top of each other. The nominal number of arcs is two for 20 GeV case.

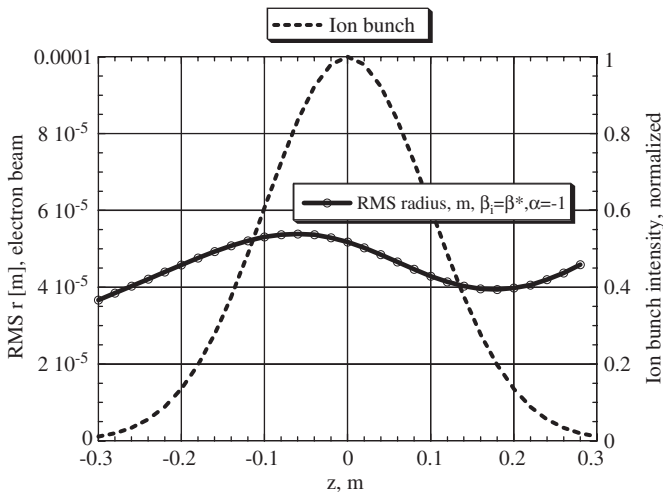


Fig. 30. Round electron beam from ERL with an initial transverse RMS emittance of 3 nm rad passes through the IP with the disruption parameter 3.61 [3] (tune shift of 0.6). The interaction with the hadron beam modifies the optic functions of electron beam significantly. The dashed line is effective density of the hadron bunch and the solid line in the size of the electron beam envelope as a function of coordinate  $z$  around the IP.

is the careful evaluation and protection of the detector from direct and scattered synchrotron radiation [36,37].

Overall, the ERL part of the eRHIC lattice has many subtle nuances but does not present significant new engineering design challenges. Many aspects of the ERL optics (e.g. the transverse and longitudinal stability) in eRHIC will be addressed in the R&D FEL as well in the e-cooler ERL. The 20 GeV ERL for eRHIC will have the same optics issues, but within a system of much larger scale.

The real challenges of these projects are in the generation of high-current electron beams with a high degree of polarization, the preservation of beam quality in the gun and merging sections, and the damping of the low-energy decelerated electron beam. Many of these issues will be addressed in the R&D ERL program at C-AD using low-energy electron guns and ERLs.

## 6. Longitudinal phase space manipulation at medium and high energy: application to energy-recovery linacs

### 6.1. Introduction

Finally in this section, we address the generic issue of longitudinal phase space evolution in an ERL which requires special attention particularly for ERLs where the quality of beam delivered is critically dependant on this single pass dynamics. To zeroth order, after the beam has been used (e.g. participated in the FEL process), has to be reinjected with the proper decelerating phase. This requires the recirculation loop to be  $\sim(n + 1/2)\lambda_{rf}$  where  $n$  is an integer and  $\lambda_{RF}$  is the wavelength associated to the radio-frequency (RF) accelerating system. To higher order, the longitudinal phase space correlations between an electron relative longitudinal coordinate<sup>1</sup>  $z$  and its fractional momentum offset  $\delta$  needs to be properly chosen such as minimizing the final fractional momentum spread after deceleration. In this note we first follow the approach presented in Ref. [13] and consider the simple case of linear longitudinal manipulation, we then build on this simple treatment and consider the effects of longitudinal space charge (LSC). We also address possible issues pertaining to CSR.

### 6.2. Linear longitudinal dynamics

We first discuss the requirement on the decelerating phase  $\phi'$  and consider an electron being accelerated by the accelerating voltage  $V_{RF}$  and phase  $\phi$ . The electron energy gain is  $\Delta\epsilon = eV_{RF} \cos \phi$ . Proper energy recovery requires the energy loss of the electron being decelerated to be opposite to the energy gain of the accelerated electron. This requirement alone imposes two values for the decelerating phase  $\phi'_{\pm} = \pi \pm \phi$ .

<sup>1</sup>In our convention  $z > 0$  corresponds to the bunch tail.

Let us now consider the requirement on the linear correlation between  $z$  and  $\delta$ . The energy gain for an electron with longitudinal coordinate  $z_A$  is  $\Delta\mathcal{E}_A(s) = eV_{\text{RF}}[\cos(kz_A + \phi) - \cos\phi]$  where  $k \doteq 2\pi/\lambda_{\text{RF}}$ . The corresponding fractional momentum spread is  $\delta_A(s) \doteq \Delta\mathcal{E}_A(s)/\mathcal{E}_A$  where  $\mathcal{E}_A = \mathcal{E}_0 + eV_{\text{RF}} \cos\phi$ . The linear correlation imparted in  $(z_A, \delta_A)$  is  $r_A \doteq d\delta_A/dz_A|_{z_A=0} = (-eV_{\text{RF}}/\mathcal{E}_A) \sin\phi$ . After acceleration, the beam propagates through a recirculation loop characterized by its overall momentum compaction  $R_{56}$ . When no source of energy spread is taken into account, the longitudinal motion due to the non-isochronicity of the loop may alter the longitudinal phase space correlation. The correlation coefficient downstream of the recirculation loop is thus given by  $r_{D^-} = r_A/(1 + r_A R_{56})$ . Similar to the acceleration, the deceleration induces a linear correlation given by  $r_D = eV_{\text{rf}}/\sin\phi'$ , where  $\mathcal{E}_D$  is the energy after deceleration. The main goal of the overall longitudinal phase space manipulation is to reduce the fractional momentum spread of the decelerated beam. Ideally, the cancellation is achieved, to first order, when

$$r_{D^-} \frac{\mathcal{E}_A^-}{\mathcal{E}_D} + r_A = 0. \quad (1)$$

Practically it is instructive to consider the two cases associated with the possible decelerating phase values  $\phi'_{\pm}$ . Case (1): the recirculation loop is isochronous  $R_{56} = 0$  and Eq. (1) is verified for  $\phi' = \phi + \pi$ . Case (2): the recirculation loop is set up as a reflector ( $r_A R_{56} = -2$  or  $z \rightarrow -z$ ) and Eq. (1) requires  $\phi' = \pi - \phi$ . These two cases are illustrated in Fig. 31. Case (2) is generally undesired since it implies the bunch is over-compressed and collective effects such as CSR might be detrimental to the beam quality (see below).

We now include in the model the effects of LSC on the correlation coefficient. This is motivated by recent observations at the JLab 10 kW FEL [38]. The topics have already been addressed in Ref. [39]. Given the on-axis longitudinal electric field associated to LSC [40], we derive the induced linear correlation in the longitudinal phase space

$$r_{\text{LSC}} \doteq \left. \frac{d\delta_{\text{SC}}}{dz} \right|_{z=0} = \frac{g_0 \hat{I}}{I_A \sigma_z^2 \gamma} \begin{cases} L/\gamma^2 \text{ for a drift} \\ L/\gamma_0 \gamma \text{ in an accelerating section.} \end{cases} \quad (2)$$

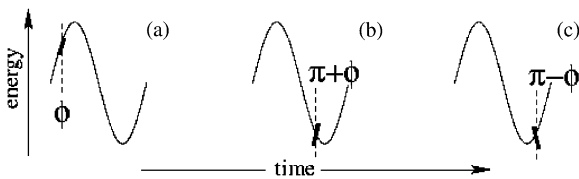


Fig. 31. Illustration of the possible phase choices for deceleration. The beam is accelerated off-crest (a), and presented at the entrance of the linac after an isochronous recirculation transport (b) and a reflecting transport (c). The heavy line represents the bunch w.r.t. the RF-wave (tail is on the right in our sign convention).

The longitudinal charge distribution is assumed to be a Gaussian with RMS length  $\sigma_z$ .  $L$  is the length of the considered section,  $g_0$  is a geometric factor,<sup>2</sup>  $I_A = 17 \text{ kA}$  is the Alfvén current and  $\hat{I} = |Q|c/(\sqrt{2\pi}\sigma_z)$  is the peak current within the bunch ( $Q$  is the bunch charge). The Lorentz factors  $\gamma$  and  $\gamma_0$  correspond, respectively, to the energy at which Eq. (2) is evaluated and to the initial energy when acceleration is considered.<sup>3</sup> LSC introduces a positive correlation in our convention: the tail (resp. head) of the bunch loses (resp. gains) energy. When the full recirculation is taken into account, the total LSC-induced change of correlation is

$$r_{\text{LSC,tot}} \approx \frac{g_0 \hat{I}}{I_A \gamma_A} \left[ 2 \frac{L_{\text{linac}}}{\sigma_{z,\text{linac}}^2 \gamma_0 \gamma_A} + \frac{L_{\text{recirc}}}{\sigma_{z,\text{recirc}}^2 \gamma_A^2} \right] \quad (3)$$

where  $\sigma_{z,\{\text{linac,recirc}\}}$  are the average bunch length in the accelerating (or decelerating) and recirculation sections, and  $L_{\text{linac,recirc}}$  are the length of the sections. Considering the numerical values experimentally achieved at the JLab 10 kW FEL [38],  $\sigma_z \approx 0.5 \text{ mm}$ ,  $Q = 135 \text{ pC}$ ,  $\gamma = 160$  assuming  $g_0 = 3$  and taking a drift length  $L = 130 \text{ m}$ , we obtain  $r_{\text{LSC}} \approx 2.3 \text{ m}^{-1}$ . The latter value translates into a needed change of  $\sim 5^\circ$  in the accelerating section phase in order to maintain the same correlation as the one that would be achieved without accounting for LSC (we assume  $\mathcal{E}_A = 80 \text{ MeV}$  and  $eV_{\text{RF}} = 71 \text{ MeV}$ ). Because of the significant impact of LSC, the matching condition (1) has to be modified by changing  $r_A$  into  $r_A + r_{\text{LSC,tot}}$ .

Practically, the recirculation transport also provides local manipulation of the longitudinal phase space. For instance, a local dispersion bump conveniently located compresses the bunch. In this case the upstream accelerating linac has to be operated off-crest. Introducing the magnetic compressor momentum compaction  $R_{56,\text{BC}}$ , the RMS bunch length after compression is related to the initial bunch length  $\sigma_{z_0}$  and relative fractional momentum spread  $\sigma_{\delta_0}$  via

$$\sigma_{z,\text{BC}} = \left[ \mu^2 \sigma_{z_0}^2 + \left( R_{56,\text{BC}} \sigma_{\delta_0} \frac{\mathcal{E}_0}{\mathcal{E}_A} \right)^2 \right] \quad (4)$$

where  $\mu = 1 + r_A R_{56,\text{BC}}$ . The remaining longitudinal lattice downstream of the bunch compressor area (e.g. after a wiggler) is set up to provide a momentum compaction opposite to the bunch compressor ( $R_{56,\text{R}} = -R_{56,\text{BC}}$ ) thereby vanishing the total momentum compaction of the recirculation loop (since  $R_{56} = R_{56,\text{R}} + R_{56,\text{BC}}$ ). Because the minimum achievable bunch length is  $R_{56,\text{BC}} \sigma_{\delta_0} (\mathcal{E}_0/\mathcal{E}_A)$ , compressing the bunch to its maximum should be avoided, especially at high energy, due to possible detrimental collective effects.

<sup>2</sup> $g_0 = 1 + 1/2 \log(b/a)$  for a transverse uniform bunch of radius  $a$  propagating in a perfectly conducting pipe of radius  $b$ .

<sup>3</sup>We assume the acceleration is of the form  $\gamma(s) = \gamma_0 + \gamma's$ , where  $\gamma' = d\gamma/ds$ .

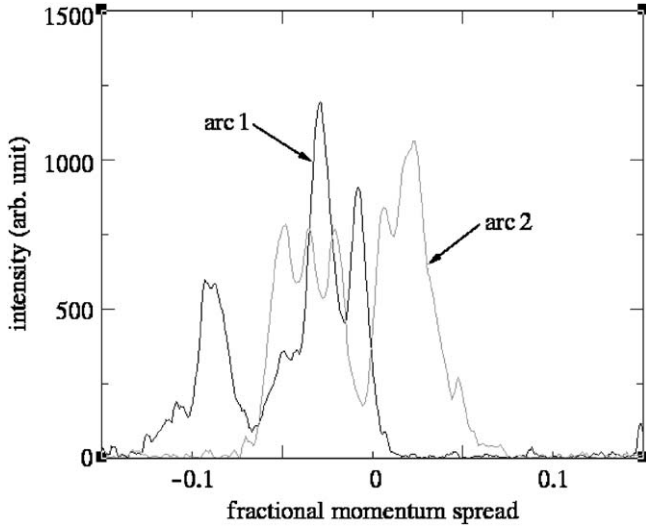


Fig. 32. Fractional momentum spread of a 60 pC bunch measured in the middle of the two 180° arcs of the IR-Demo [measurement by P. Piot (July 1999)]. The origin of the horizontal axis is arbitrary.

In the JLab IR-Demo, the bunch was going through three longitudinal waists during the recirculation [41], and despite the relatively low energy ( $\mathcal{E} = 40$  MeV) and modest uncorrelated energy spread ( $\mathcal{E}\sigma_{\delta_0} \approx 5$  keV), significant energy modulation at 60 pC was observed; see Fig. 32.

### 6.3. Nonlinear effects and cures

The linear approach in the previous section breaks as soon as sources of momentum spread dilutions, e.g. induced by the FEL process, are included. The resulting large fractional momentum spread (and thus the longer bunch after deceleration) requires the previous treatment to include second and possibly higher-order terms in  $z$ . Nonlinear effects should indeed be included starting from upstream of the injector especially since in common present injector designs the bunch is kept long in order to mitigate transverse emittance growth due to space charge. Then, during acceleration in the linac, the longitudinal phase space accumulates nonlinear correlations introduced by the cosine-like dependence of the accelerating field ( $kz$  much less than 1 is not satisfied). The fractional momentum spread, including second order in  $z$ , is

$$\delta_A(z_A) = r_A z_A + t_A z_A^2 + O(z_A^3) \quad (5)$$

where  $t_A = (1/2)(d^2\delta_A/dz^2)$ . When the beam is compressed using magnetic compression, the longitudinal coordinate becomes  $z_a \rightarrow z_{BC} = z_A + R_{56,BC} \delta_A + T_{566,BC} \delta_A^2$  ( $T_{566,BC}$  is the second-order momentum compaction), and the final RMS bunch length becomes

$$\sigma_{z,BC} = [\mu^2 \sigma_{z_0}^2 + v^2 \langle z_A^4 \rangle + 2\mu v \langle z_A^3 \rangle + R_{56,BC}^2 \langle \delta_{A,u}^2 \rangle + T_{566,BC}^2 \langle \delta_{A,u}^4 \rangle]^{1/2} \quad (6)$$

where  $v \equiv t_A R_{56,BC} + r_A^2 T_{566,BC}$  and  $\delta_{A,u}$  is the stochastic fractional momentum spread. The distortion imposed by

the second-order effects impacts the charge density profile [42] and results in a larger RMS bunch length (see Fig. 33). The second-order contribution on the bunch compression can be suppressed provided  $\mu = 0$ . At medium or high energies<sup>4</sup> two possible alternatives for canceling  $\mu$  are (1) design a bunch compressor with proper  $R_{56,BC}/T_{566,BC}$  ratio, or (2) locally linearize the longitudinal phase space by using a harmonic RF accelerating section operated on a decelerating phase [44,45]. The first solution requires a bending system that provides the same sign for  $R_{56,BC}$  and  $T_{566,BC}$ . This requirement can be implemented, e.g. with FODO-type arc that includes sextupoles, but cannot be met with a standard four-dipoles chicane. In the case of local linearization of the phase space, the harmonic RF section allows an independent control of the coefficients  $r_A$  and  $t_A$  [46]. In the latter case the second-order correlation coefficient  $t_A = -ek^2/\mathcal{E}_A (V_{RF} \cos \varphi + V_{RF,m} m^2 \cos \varphi_m)$  (where  $m \in \mathbb{N}$  is the harmonic number) can be zeroed by a proper choice of the operating parameters  $V_{RF,m}$  and  $\varphi_m$  of the harmonic accelerating section. The introduction of a harmonic RF section is generally preferred since it has the advantage, compared to a tailored dispersive section, not to introduce coupling between the longitudinal and transverse phase spaces. In the case of ERLs operating at the TESLA frequency ( $f = 1.3$  GHz), a third harmonic accelerating cavity ( $f = 3.9$  GHz) has been developed at Fermilab [47] and will soon be installed in the injector [48] of the TESLA vacuum ultra-violet FEL at DESY.

If the compression is set up to perform linearly, e.g. by using a higher-order harmonic section, the final fractional momentum spread after deceleration is

$$\delta_D = \delta_W \left( \frac{\varepsilon_W}{\varepsilon_D} + R_{56,R} r_D \right) + \delta_W^2 (r_D T_{566,R} + t_D R_{56,R}^2) \equiv \bar{\mu} \delta_W + \bar{\nu} \delta_W^2,$$

where  $R_{56,R}$  and  $T_{566,R}$  are the parameters associated to the recirculation transport downstream of the bunch compressor, the subscript W refers to the parameters after the wiggler, and  $r_D$  and  $t_D$  are the linear and quadratic correlations induced by the deceleration. Since the path length is properly set to have  $\varphi' = \pi + \varphi$ , we have the relations  $(r_D, t_D) = -(r_A, t_A) \mathcal{E}_A / \mathcal{E}_D$ . The condition  $\bar{\mu} = 0$  is satisfied de facto when  $R_{56,BC} = -R_{56,R}$  and provided the energy loss induced by the FEL process is small compared to  $\varepsilon_A$ . The condition  $\bar{\nu} = 0$  requires  $T_{566,R} = -t_A T_{566,BC}$ .

### 6.4. Summary

So to summarize in this section, a presentation has been made in detail of the issues to be considered to achieve optimized LSC profiling for the application of ERLs. This has included covering the important issue of bunch compression which for designs dependent on delivering

<sup>4</sup>At non-relativistic energies, nonlinear compression can be used to linearize the phase space [43].

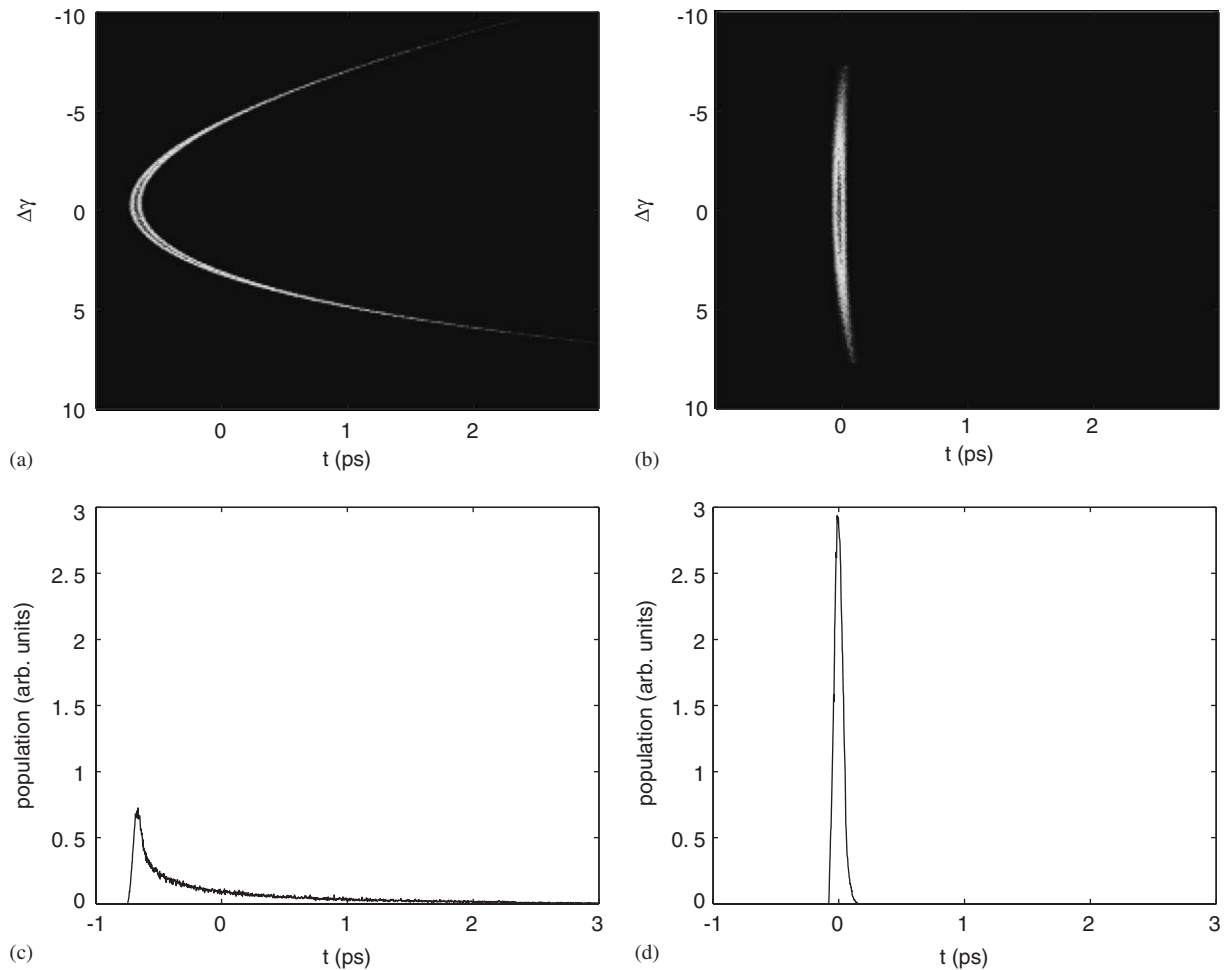


Fig. 33. Longitudinal phase space after compression without (a) and with (b) linearization of the longitudinal phase space prior to the bunch compressor. The profile (c) and (e), respectively, corresponds to the charge density associated to (a) and (b).

high-quality intense bunches with femtosecond duration is extremely important.

## 7. Summary

The projects used to illustrate how optics issues influence design, cover a range of energies and applications at various stages and are at various stages of delivery. This has presented a wide overview of disparate issues regarding the optics design. The presentation of longitudinal dynamics issues in Section 6 illustrates how despite their differences there are a number of issues that are fundamental to ERL project design as a whole and illustrates that these can be usefully studied and understood at a more generic level.

## Acknowledgements

The sections on the 4GLS and ERLP projects at Daresbury represent the work of very many project staff at Daresbury. We have benefited from many UK and international advisors to the project. Work is funded by CCLRC and the UK Office of Science and Technology.

The work reported under Section 5, Optic Issues of ERL Projects at BNL was performed under the auspices of the US Department of Energy and partially funded by the US Department of Defense.

## References

- [1] M.W. Poole, E.A. Seddon, 4GLS and the Prototype Energy Recovery Linac Project at Daresbury, EPAC'04, Lucerne.
- [2] J.A. Clarke, et al., Prospects for a 4th Generation Light Source for the UK, PAC'01, Chicago.
- [3] M.W. Poole, et al., 4GLS: an Advanced Multi-source Low Energy Photon Facility for the UK, EPAC'02, Paris.
- [4] M.W. Poole, et al., 4GLS: a new type of 4th Generation Light Source Facility, PAC'03, Portland.
- [5] M. Borland, Elegant: a flexible SDDS-compliant code for accelerator simulation, APS LS-287, September 2000.
- [6] T. Siggins, et al., Nucl. Instr. and Meth. A 475 (2001) 549.
- [7] A. Baeuchner, et al., The ELBE-Project at Dresden-Rossendorf, EPAC'00, Vienna, June 2000.
- [8] C. Gerth, F.E. Hannon, Injector design for the 4GLS Energy Recovery Linac Prototype, EPAC'04, Lucerne, July 2004.
- [9] S.B. van der Geer, O.J. Luiten, M.J. de Loos, G. Poeplau, U. van Rienen, 3D space-charge model for GPT simulations of high-brightness electron bunches, in: M. Berz, K. Makino (Eds.),

- Computational Accelerator Physics 2002, Institute of Physics Conference Series No. 175, p. 101, 2005 and [www.pulsar.nsl.gov](http://www.pulsar.nsl.gov)
- [10] K. Floettmann, ASTRA User Manual, September 18, 2000, <http://www.desy.de/~mpyflo>
- [11] N. Vinokurov, Space charge, in: Proceedings of the Joint US-CERN-JAPAN-RUSSIA Accelerator School, St. Petersburg and Moscow, Russia, 2000.
- [12] B.D. Muratori, H.L. Owen, C.K.M. Gerth, S.B. van der Geer, M.J. de Loos, Space charge effects for the ERL prototype injector line at Daresbury Laboratory, PAC'05, Knoxville, May 2005.
- [13] P. Piot, D.R. Douglas, G.A. Krafft, Phys. Rev. S.T. Accel. Beams 6 (2003) 030702.
- [14] I.V. Bazarov, C.K. Sinclair, Multivariate optimization of high brightness photoinjectors, in preparation, 2005.
- [15] H. Padamsee, et al., An overview of the cryomodule for the Cornell ERL injector, in: Proceedings of EPAC04, 2004.
- [16] I.V. Bazarov, Overview of energy recovery linacs, in: Proceedings of PAC05, 2005.
- [17] G.H. Hoffstaetter, et al., The Cornell ERL prototype project, in: Proceedings of PAC03, Portland, OR, 2003.
- [18] S.M. Gruner, M. Tigner (Eds.), Phase I ERL synchrotron light source at Cornell University, Report CHESS-01-003.
- [19] I.V. Bazarov, G.H. Hoffstaetter, Lattice options for a 5GeV light source at Cornell, in: Proceedings of PAC03, Portland, OR, 2003.
- [20] I.V. Bazarov, G.H. Hoffstaetter, Multi-pass beam-breakup: theory and calculation, in: Proceedings of EPAC04, 2004.
- [21] C. Tennant, et al., Experimental investigation of beam breakup in the Jefferson Laboratory 10kW REL upgrade, in: Proceedings of PAC05, 2005.
- [22] G.H. Hoffstaetter, et al., A lattice for a 5GeV ERL in the CESR tunnel, in: Proceedings of PAC03, Portland, OR, 2003.
- [23] I. Ben-Zvi, Ya Derbenev, V.N. Litvinenko, L. Merminga, Energy recovery linacs in high-energy and nuclear physics, Nucl. Instr. and Meth. A, these proceedings, doi:10.1016/j.nima.2005.10.057.
- [24] M. Harrison, et al., Special issue of Nucl. Instr. and Meth. A 499 (2–3) (2003), <http://www.physicstoday.org/vol-56/iss-10/p48.html>
- [25] W. MacKay, I. Ben-Zvi, J.M. Brennan, M. Harrison, J. Kewisch, S. Peggs, T. Roser, D. Trbojevic, V. Parkhomchuk, Upgrading RHIC for higher luminosity, in: Proceedings of PAC'2001, Chicago, IL, USA June 18–22, 2001, <http://www.agsrhichome.bnl.gov/eRHIC/>
- [26] D. Anderson, I. Ben-Zvi, R. Calaga, X. Chang, M. Farkhondeh, A. Fedotov, J. Kewisch, V. Litvinenko, W. Mackay, C. Montag, T. Roser, V. Yakimenko, [http://www.agsrhichome.bnl.gov/eRHIC/eRHIC\\_ZDR/AppendixA.pdf](http://www.agsrhichome.bnl.gov/eRHIC/eRHIC_ZDR/AppendixA.pdf)
- [27] V.N. Litvinenko, et al., in: Proceedings of the 2004 FEL Conference, p. 570, <http://accelconf.web.cern.ch/AccelConf/f04>
- [28] V.N. Litvinenko, D. Kayran, R. Hajima, Merger designs for ERLs, Nucl. Instr. and Meth. A, These Proceedings, ERL 2005, Newport News, VA, doi:10.1016/j.nima.2005.10.065.
- [29] R. Calaga, et al., High current superconducting cavities at RHIC, TUPKF078, in: Proceedings of EPAC-2004, Geneva, Switzerland, July 5–9, 2004.
- [30] L.M. Young, J.H. Billen, Parmela documentation, LA-UR-96-1835.
- [31] Zero design report on electron cooling of RHIC, edited by M. Farkhondeh and V. Ptitsyn, <http://www.agsrhichome.bnl.gov/eCool/>
- [32] J. Kewisch, I. Ben-Zvi, X. Chang, Electron beam generation and transport for the RHIC electron cooler, in: Proceedings of 2005 Particle Accelerator Conference, May 16–20, 2005, Knoxville, TN, USA.
- [33] R. Brinkmann, Ya Derbenev, K. Floettmann, Phys. Rev. ST Accel. Beams 4:053501, 2001.
- [34] J. Kewisch, et al., in: Proceedings of the 2003 Particle Accelerator Conference, Portland, OR, USA, May 12–16, 2003, p. 2007 <http://accelconf.web.cern.ch/accelconf/p03/PAPERS/WPAE028.PDF>
- [35] C. Montag, et al., Interaction region design for the electron-ion collider eRHIC, in: Proceedings of 2005 Particle Accelerator Conference, May 16–20, 2005, Knoxville, TN, USA.
- [36] J. Beebe-Wang, et al., Synchrotron radiation in eRHIC interaction region, in: Proceedings of 2005 Particle Accelerator Conference, May 16–20, 2005, Knoxville, TN, USA.
- [37] B. Surrow, eRHIC detector design studies—implications and constraints on the ep(A) interaction-region design, in: Proceedings of 2005 Particle Accelerator Conference, May 16–20, 2005, Knoxville, TN, USA.
- [38] C. Hernandez-Garcia, et al., in: Proceedings of FEL 2004, 2004, p. 363.
- [39] H. Liu, Nucl. Instr. and Meth. A 400 (1997) 213.
- [40] A.W. Chao, Physics of Collective Beam Instabilities in High Energy Accelerators, Wiley, New York.
- [41] D.R. Douglas, et al., in: Proceedings of PAC 2003, 2003, p. 213.
- [42] R. Li, Nucl. Instr. and Meth. A 475 (2001) 498.
- [43] G.A. Krafft, in: Proceedings of micro bunches workshop, AIP Conference Proceeding No. 367, 1996, p. 46.
- [44] T. Smith, in: Proceedings of LINAC 1984, SLAC Report 303, 1986.
- [45] Dowell, et al., Nucl. Instr. and Meth. A 375 (1996) 108.
- [46] K. Floettmann, et al., DESY report TESLA-FEL-2001-06, 2001.
- [47] N. Solyak, et al., in: Proceedings of LINAC 2004, 2004, p. 797.
- [48] K. Floettmann, P. Piot, in: Proceedings of EPAC 2002, 2002, p. 1798.